chemosensors

MDPI

Review

Rational Design Copper Nanocluster-Based Fluorescent Sensors towards Heavy Metal Ions: A Review

Lili Yuan [1,†], Mengna Liang [1,†], Matthew Hummel [2], Congying Shao [1,*] and Shun Lu [3,4,*]

[1] Key Laboratory of Green and Precise Synthetic Chemistry, Ministry of Education, College of Chemistry and Materials Science, Huaibei Normal University, Huaibei 235000, China
[2] Biochemistry R&D, Neogen Corporation, Lansing, MI 49812, USA
[3] Department of Agricultural and Biosystems Engineering, South Dakota State University, Brookings, SD 57007, USA
[4] Chongqing Institute of Green and Intelligent Technology, Chinese Academy of Sciences, Chongqing 400714, China
* Correspondence: shaocongying@163.com (C.S.); lushun@cigit.ac.cn (S.L.)
† These authors contributed equally to this work.

Abstract: Recently, copper nanoclusters (CuNCs) have attracted great research interest for their low synthesis cost, wide application, and easy functionalization. Until now, CuNCs have been developed and applied in multi-fields such as sensing, catalysis, light-emitting diode manufacturing, and cell imaging. Furthermore, the application of heavy metal ions (HMIs) detection is also regarded as a major part of fluorescence sensing and the necessity of detecting the makeup of HMIs (Ag^{+}, Te^{3+}, Co^{2+}, Se^{6+}, Hg^{2+}, Mn^{2+}, etc.) in organisms and the environment. This has promoted the development of CuNCs in fluorescence sensing. This paper reviews the research progress of CuNCs detection in HMIs, which can be divided into four parts. The synthesis and characterization of CuNCs are first described. Then, the synthesis methods making the types of CuNCs more varied are also summarized. Furthermore, mechanisms of fluorescence changes induced by HMIs are explained. After that, the relevant reports of CuNCs in several typical HMI detection are further listed. In addition, combined with the above content, the challenges and prospects of CuNCs in HMIs detection are also proposed.

Keywords: copper nanoclusters; fluorescent sensors; heavy metal ions; nano probes; detective mechanism

check for updates

Citation: Yuan, L.; Liang, M.; Hummel, M.; Shao, C.; Lu, S. Rational Design Copper Nanocluster-Based Fluorescent Sensors towards Heavy Metal Ions: A Review. *Chemosensors* **2023**, *11*, 159. https://doi.org/10.3390/chemosensors11030159

Academic Editor: Ambra Giannetti

Received: 31 January 2023
Revised: 22 February 2023
Accepted: 22 February 2023
Published: 25 February 2023

Copyright: © 2023 by the authors. Licensee MDPI, Basel, Switzerland. This article is an open access article distributed under the terms and conditions of the Creative Commons Attribution (CC BY) license (https://creativecommons.org/licenses/by/4.0/).

1. Introduction

In the typical definition, heavy metals are metals whose atomic weights ranging from 63.5 to 200.6 $g \cdot mol^{-1}$ and have a specific gravity above 5 $g \cdot cm^{-3}$ [1]. They are a kind of micropollutant that can be released into the environment through industrial processes, the burning of fossil fuels, fertilizers, domestic waste, etc. Heavy metals will pollute the environment and affect the life activities of organisms when their content reaches a certain level. They can enter and accumulate in organisms through various pathways such as the respiratory tract, food intake, and skin contact [2,3]. The presence of heavy metals can have serious impacts on life and the environment. For example, excessive amounts of copper can cause vomiting, cramps, and seizures. High levels of mercury can impair lung and kidney function, and even cause respiratory problems [4]. Manganese in water has been linked to poor concentration in children and neurotoxicity in people over 50. In addition, high levels of manganese may produce impaired neuromuscular control and nervous systems [5]. However, even trace amounts of lead, cadmium, arsenic, and mercury are highly toxic, compromising organisms and their ecosystems [3]. Therefore, it is necessary to monitor and control the content of heavy metal ions (HMIs) due to the serious impact on the environment and organisms.

For the detection of HMIs, the commonly used methods include colorimetric methods, fluorescence methods, electrochemical methods [6,7], point-of-care testing (POCT), etc., [3,8]. Colorimetric methods are used to determine the analyte composition by comparing or measuring the color intensity of a colored substance [9]. Using electrochemical methods to design sensors can improve performance by creating novel substrates with large surface areas [10–13], good chemical stability [14–16], and high electrical conductivity [17–20]. Among the above listed methods, fluorescence methods have several advantages of being fast, simple, and convenient, which can satisfy common basic analytical requirements. Fluorescence is a form of luminescence, a phenomenon in which excited atoms or molecules emit light spontaneously. The change in fluorescence of the substance is used to complete the detection. The first fluorometric sensor was developed by Friedrich Goppelsroder in 1867 and was used to detect Al^{3+} by forming a compound with strong fluorescence [21]. Since then, fluorescent sensors that achieve metal ion detection have come into view.

Metal nanoclusters (MNCs) are small organic aggregates, usually less than 3 nm in diameter [22,23]. For the past few decades, the breakthrough in the synthesis of MNCs at the molecular and atomic levels had laid a strong foundation for obtaining high-purity MNCs [23]. MNCs had developed rapidly in the last decade due to their high photoluminescence and quantum yield. Various fluorescent MNCs have been prepared that can be used as a probe for sensing [24]. Over the past years, significant advances had been made in the synthesis and application of MNCs due to their optical and electronic properties [25,26]. MNCs fabrication methods included direct reduction, chemical etching, and so on [27]. They also had promising applications in the fields of sensing, biomedicine, catalysis, and light-emitting diodes due to the above-mentioned merits [28]. The wide variety of raw materials used for the synthesis of nanomaterials, including biomacromolecules, amino acids, DNA, enzymes, and some biomass materials [29] expanded the types of MNCs investigations.

Copper nanoclusters (CuNCs) have the advantages of high luminous efficiency, long fluorescent life, good optical stability, and large stokes shift [30]. Compared with semiconductor quantum dots and many organic dyes, CuNCs are relatively weak in brightness, and their stability has a strict requirement for environmental conditions [24]. The quantum yield (QY) is relatively low compared to other MNCs [30]. However, compared with gold or silver nanoclusters, Cu is rather inexpensive and more readily available in nature, making CuNCs more attractive for sensor development [31]. The fluorescence sensor designed with CuNCs as a fluorescent probe has high sensitivity, accuracy, short response time, and low cost [32]. Fluorescent colors can be easily observed with the assistance of a smartphone. Designed as a portable fluorescent sensor, it can be used in complex environments to perform tests quickly and accurately [33,34].

Although a few review articles have discussed CuNCs, most tend to focus on synthesis, performance, and structure [24,35]. The application of CuNCs focuses on biological imaging and the detection of various substances [35,36]. However, as for the application potential of CuNCs, this review discusses in detail the detection of HMIs. Figure 1 briefly summarizes the discussion process of this paper. First, the synthesis methods, such as the template-assisted method, ligand-capped method, and etching method are introduced. Then, the characterization method of CuNCs and the detection mechanism of CuNCs as fluorescent probes were analyzed. Following, some reports of HMIs detection with CuNCs are listed. Finally, the review ends with the development prospects and challenges of CuNCs.

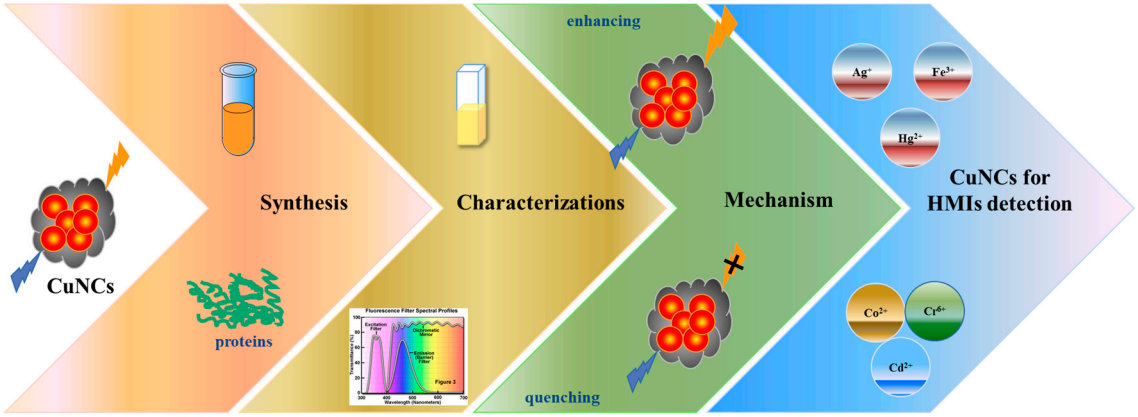


Figure 1. Summary of CuNCs and HMIs detection applications.

2. Synthesis of Fluorescent Copper Nanoclusters

Due to the sensitivity of CuNCs to oxidation, the primary difficulty of synthesis is to prepare stable CuNCs [35,37]. Recently, some methods have been developed to overcome this difficulty. Several common synthetic methods are described below, including the template-assisted method, ligand-capped method, etching method, and copper-included bimetallic NCs (Figure 2).

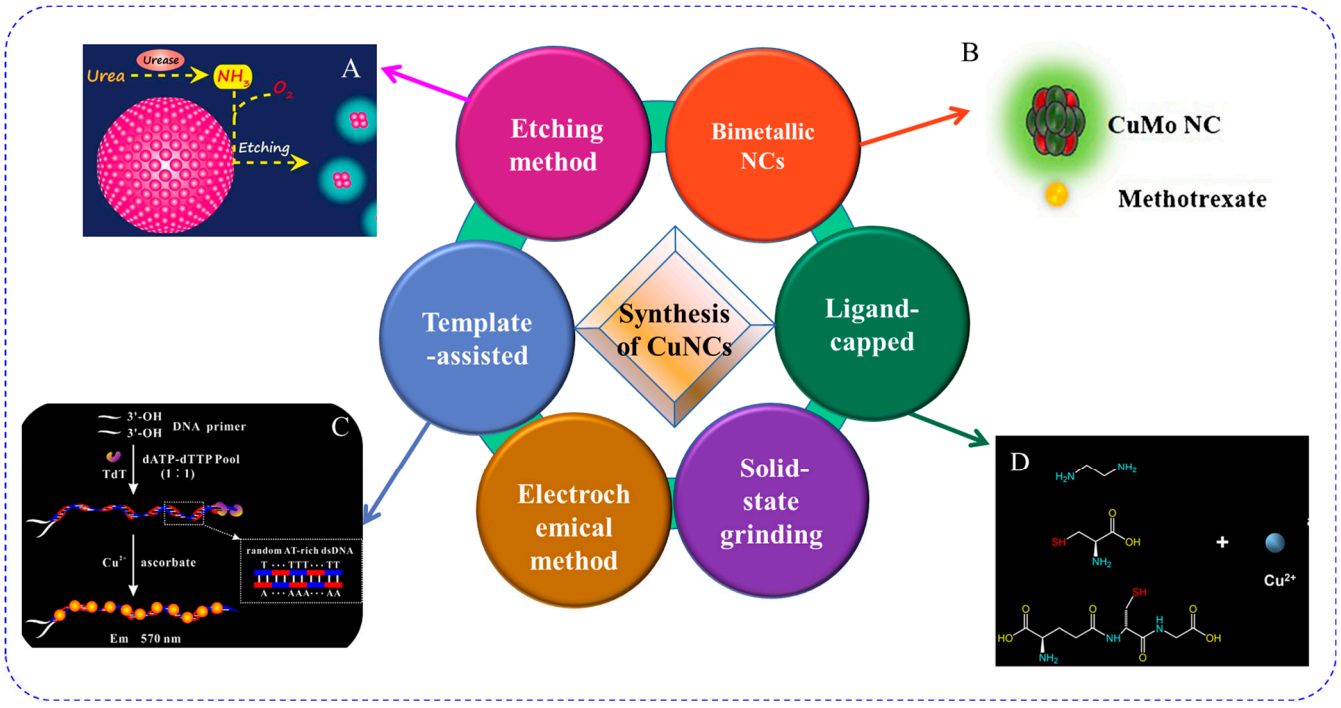


Figure 2. (**A**) Etching method: NH_3 triggered fluorescence generation [38], Copyrights from Royal Society Chemistry, 2018. (**B**) Copper-included bimetallic NCs: Cu/Mo bimetallic NCs [39], Copyrights from Springer, 2019. (**C**) Examples of the template-assisted method [40], Copyrights from Springer, 2017. (**D**) Ligand-capped method: small molecule as a capped ligand [41], Copyrights from Springer, 2020.

2.1. Template-Assisted Method

The template-assisted method can use proteins, peptides, enzymes, DNA, and polymers as templates. The advantage of this method is that different templates can be used to form NCs with different size distributions [37]. First discussed is the use of protein as a template. Lettieri et al. proposed using human serum albumin (HSA) as the tem-

plate to prepare HSA-CuNCs [42]. HSA-CuNCs were generated by repeated growth of CuNCs directly on HSA and produced fluorescence emission at 405 nm. Second, using DNA as a template. In the process of synthesis, DNA templated-CuNCs were prepared using terminal deoxyriboside transferase (TdT) polymerized long-chain AT-rich DNA as a template [40]. Using CuNCs as the probe, the activity of TdT was measured by the change in fluorescence intensity. The synthesis with DNA as the assisted template has high efficiency and low difficulty (Figure 2C). In addition, there is another work detailing the synthesis of CuNCs using peptides as a template for the detection of Fe^{3+} in human serum [43]. The polypeptide template in the experiment was Cys-Cys-Cys-Asp-Leu. The presence of Fe^{3+} oxidized CuNCs, leading to fluorescence quenching. The template-assisted method possesses significant advantages, such as easy-to-synthesis, controllable size and morphology, even brings good biocompatibility, making CuNCs as emerging candidates in biological fields. However, the selection of templates is vital important for the properties of the as-prepared CuNCs. Exploring proper templates to synthesis the desired CuNCs is also noteworthy.

2.2. Ligand-Capped Method

There are also various methods to synthesize CuNCs using amino acids or other small molecules as capped ligands. The presence of ligands can protect and stabilize the CuNCs [44]. A recent report used tryptophan (Trp) as a reducing agent and a capping agent to synthesize CuNC@Trp [45]. NaOH was added in the synthesis process and the negatively charged ligand had stronger adhesion to copper ions when the isoelectric point of tryptophan was higher. As a result, the stability of the synthesized NCs was improved. Luo et al. introduced the use of ethylenediamine as a capped ligand to form fluorescent probes [41] and discussed the connection between luminescence color and ligand through three ligands (Figure 2D). The binding ability of the ethylenediamine ligand is weak, but the CuNCs with ethylenediamine as the ligand has strong emission and stable fluorescence, which can be directly used for Hg^{2+} detection.

2.3. Etching Method

The etching method refers to the use of chemical methods to process nanoparticles (NPs) to form smaller NCs [46]. The etching technique can adjust the size of the NCs [47]. In a chemical etching process, Yan et al. constructed CuNCs using ascorbic acid as a reducing agent and protective agent [48]. The Cu nanocrystals were spherical and uniform in size distribution. Under the corrosion of the NaOH solution, Cu nanocrystals were rapidly decomposed into small fluorescent NCs with a QY of 33.6%. After the conditions were optimized, the pH of the solution was about 8–9. Another interesting work described the synthesis of luminescent CuNCs using copper nanoparticles (CuNPs) as the precursor and ammonia (NH_3) as the etching agent [38]. In the presence of NH_3 and dissolved oxygen in the solution (Figure 2A), the etching reaction was activated, and the etching process was very fast. After etching, the CuNCs was smaller in size compared to the CuNPs. The newly synthesized CuNCs had green fluorescence and a QY of 6.63%.

2.4. Copper-Included Bimetallic Nanoclusters

Because of the doping of atoms, the composition and electronic structure of bimetallic nanoclusters change, which affects their fluorescence properties and catalytic activities. Yang et al. demonstrated that the presence of heteroatoms plays a positive role in the fluorescence characteristics of AgNCs, and also has more potential for catalytic applications [49]. Synthesis and application of bimetallic NCs composed of copper and other metals have been reported and widely used in the field of sensing. In one report, Cu/Mo bimetallic NCs (Figure 2B) were prepared using cysteine as a capping agent and NaOH as a reducing agent for the determination of methotrexate [39]. The luminescence intensity of bimetallic NCs was higher than that of single MNCs of copper and molybdenum. These NCs can concentrate the properties of the two metals and achieve intense luminescence [50].

2.5. Other Methods

In addition to the synthesis methods of CuNCs discussed above, there are many other methods. For example, electrochemical methods, solid-state grinding methods, etc. In previous work, reduced graphene oxide (RGO) and copper nanodendrites (Cu-NDs) were deposited sequentially on a glass carbon electrode by two-step electrodeposition [51]. Based on this, a kind of enzyme-free nitrite sensor was developed. Electrodeposition disperses Cu-NDs on RGO, which means that RGO provides a platform for the deposition of Cu-NDs. By the electrochemical method, the current density can be adjusted to obtain high-purity CuNCs with a certain particle size [37]. In addition, fluorescent CuNCs were also prepared by the solid-state grinding method. The solid-state grinding method has the advantages of being green and simple. Liu et al. used a simple solid-state grinding method to produce silver nanoparticles to detect Al^{3+}, with a detection limit (LOD) of 0.1 uM [52]. After the mixed grinding of $AgNO_3$ and glutathione was completed, $NaBH_4$ and ultra-pure water were added successively and continued grinding. Then, after a series of simple operations such as washing, drying, dissolution, and centrifugation, silver nanoparticles are finally synthesized. This is a simple example of the synthesis of a fluorescent probe with the solid-state grinding method.

3. Characterizations of Fluorescent Copper Nanoclusters

At present, the common characterization methods for CuNCs are the following: steady and transient state fluorescence, Ultraviolet-visible (UV-vis) absorption spectroscopy, UV-vis diffuse reflectance spectra (UV-vis DRS), transmission electron microscopy (TEM), and high-resolution TEM (HR-TEM), scanning electron microscopy (SEM), field emission SEM (FE-SEM), Fourier transform infrared (FT-IR), and X-ray photoelectron spectroscopy (XPS). In addition, other characterization techniques are also involved, including thermogravimetric analysis (TGA), powder X-ray diffraction (XRD), inductively coupled plasma atomic spectrometry (ICP-AES), and Energy Dispersive X-ray (EDX) analysis. Prior to introducing the common characterization of fluorescent CuNCs, several basic concepts appeared in fluorescent data should be known, as follows: (i) Fluorescence lifetime, it is also the characteristic time that a molecule remains in an excited state prior to returning to the ground state and is an indicator of the time available for information to be gathered from the emission profile. (ii) Fluorescence decay time, the decay of fluorescence intensity as a function of time in a uniform population of molecules excited with a brief pulse of light is described by an exponential function (Equation (1)):

$$I_t = I_0 e^{-t/\tau} \tag{1}$$

where I_t is the fluorescence intensity measured at time t, I_0 is the initial intensity observed immediately after excitation, and τ is the fluorescence lifetime. The fluorescence decay time is typically on the order of nanoseconds, but some materials have much longer-lived emissions, on the order of microseconds or longer. (iii) Quantum yield, (sometimes termed quantum efficiency) is a gauge for determining the efficiency of fluorescence emission relative to all possible pathways for relaxation and is generally expressed as the ratio of photons emitted to the number of photons absorbed, as below Equation (2).

$$Q_c = Q_R \frac{I_C}{I_R} \frac{A_R}{A_C} \frac{n_C^2}{n_R^2} \tag{2}$$

where Q is the quantum yield, I is the integrated emission intensity, A is the absorbance at the excitation wavelength and n represents the refractive index of the solvent. The subscript 'R' and 'C' stand for standard with known quantum yield and the sample, respectively. The fluorescence quantum yield of MNCs, which are critical to their biological applications, are required to be measured accurately.

3.1. Steady and Transient State Fluorescence

For fluorescent materials, steady-state fluorescence spectroscopy is not only the most basic but also the vital means of characterization. Fluorescent CuNCs can be characterized by fluorescence spectrophotometer to obtain comprehensive optical properties. In the work of Shao et al., the characterization of steady-state fluorescence was used to determine the maximum excitation and emission wavelength of the prepared fluorescent nanomaterials [53]. As shown in Figure 3A, the maximum excitation and emission wavelengths of 2-mercapto-1-methylimidazole (MMI)-CuNCs are 322 and 476 nm, respectively, which corresponds to blue fluorescence under the 365 nm UV lamp. Generally, we investigate the excitation wavelength dependence of the as-synthesized CuNCs. Examining CuNCs synthesized with L-methionine (L-Met) for a template as an example (Figure 3B), the emission peak position of CuNCs/Met is basically unchanged in the range of excitation wavelength from 290 to 390 nm [54]. Thus, proving that CuNCs/Met does not have excitation wavelength dependence, indicating that the size distribution of CuNCs designed is uniform. In addition, the steady-state fluorescence spectrum also plays a crucial role in CuNCs applications, providing further support for applications, especially in sensing. Shao et al. constructed the CDs (Y-CDs) based on yeast powder for dopamine hydrochloride (DA) sensing [55]. As revealed in the fluorescence spectra (Figure 3C), the intensity of the emission peak gradually decreased with the increase of DA concentration from 0 to 250 μM, which verified the application of steady-state fluorescence characterization in sensing. Furthermore, the transient fluorescence measurement technology also plays an important role in exploring the sensing mechanism, which is usually reflected in exploring the fluorescence lifetime of materials. Typically, time-correlated single photon counting (TCSPC) is used to measure the fluorescence lifetime. As displayed in Figure 3D, the ratio of fluorescence lifetime of Y-CDs before and after adding DA is close to 1, so the fluorescence quenching mechanism was attributed to static quenching [55].

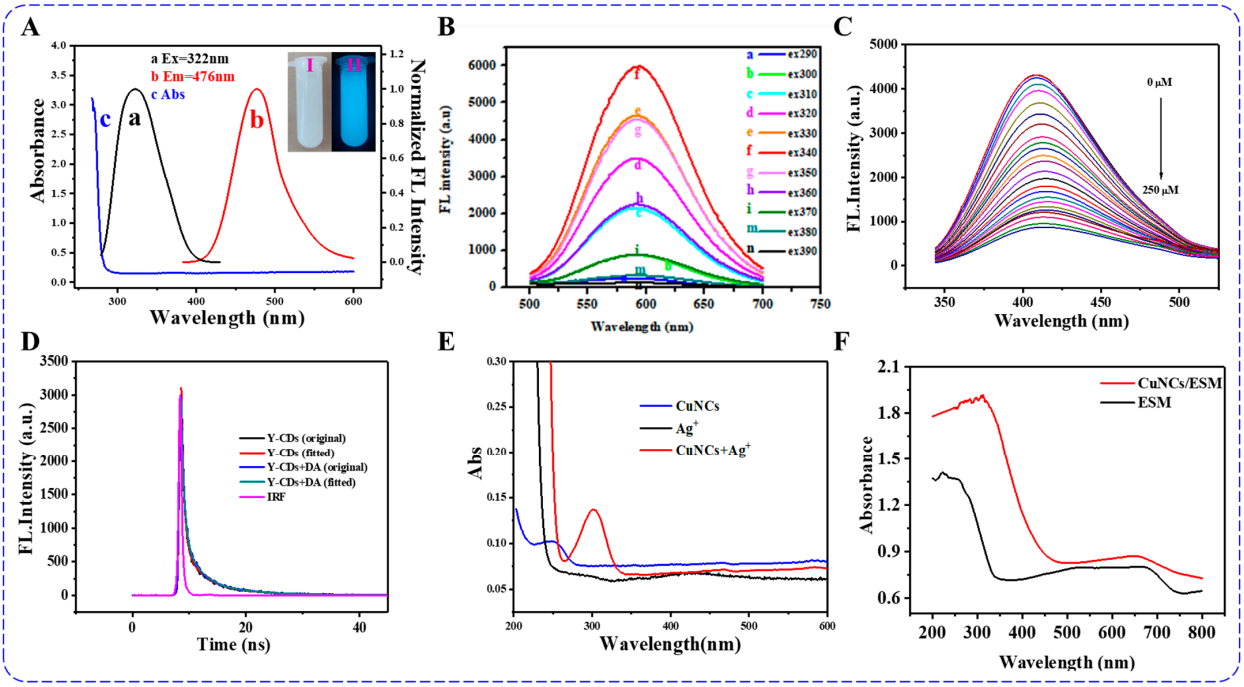


Figure 3. (**A**) Excitation and emission spectra of MMI-CuNCs (illustration: photos of MMI-CuNCs under daylight and UV lamp) [53], Copyrights from American Chemistry Society, 2022. (**B**)The emission

spectra of CuNCs/Met changing with the excitation wavelength increasing from 290 nm to 390 nm [54], Copyrights from Elsevier, 2020. (**C**) Fluorescence spectra of Y-CDs changing with the increased concentration of DA [55], Copyrights from Royal Society Chemistry, 2022. (**D**) Life decay curves of Y-CDs and other controls [55], Copyrights from Royal Society Chemistry, 2022. UV-vis absorption spectra of MMI-CuNCs (**E**) [53], Copyrights from American Chemistry Society, 2022; and UV-vis DRS spectra of CuNCs/ESM (**F**) [56], Copyrights from Springer, 2019.

3.2. UV-Vis and UV-Vis DRS

UV-vis absorption spectrum is an indispensable means to judge the formation of CuNCs. Unlike large-sized copper nanoparticles (CuNPs), which have surface plasmon resonance (SPR) absorption in the 500–600 nm band, Cu NCs exhibit molecular-like optical transitions due to their discrete electronic structures and quantum confinement effects, as well as their absorbance bands range from 216 to 468 nm [57]. For instance, the UV-vis absorption spectrum of MMI-CuNCs has an absorption peak near 248 nm (Figure 3E) [53]. Although the UV-vis absorption spectrum has the merits of good reproducibility, high accuracy, and convenience, it is not applicable to some insoluble and opaque substances. Generally, UV-vis DRS is used to characterize CuNCs in a solid state. In the work of in-situ synthesis of CuNCs based on the eggshell membrane (ESM) [56], UV-vis DRS was used to demonstrate the successful fabrication of CuNCs/ESM (Figure 3F).

3.3. Characterization of Morphology and Size

Typically, TEM and SEM are used to characterize the size and morphology of CuNCs with different states. As shown in Figure 4A, the TEM image of MMI-CuNCs shows that they are small in size and well dispersed [53]. In addition, the HR-TEM image of MMI-CuNCs (Figure 4B) shows that the lattice spacing is about 0.22 nm, which is consistent with the (111) crystal plane of Cu. Distinctively, solid CuNCs usually use SEM and FE-SEM to characterize their morphology and size. Pan et al. designed CuNCs in-situ synthesized on poly-L-Cys film and characterized it by SEM (Figure 4C) [58]. The results show that the pore structure of poly-L-Cys film corresponds to the confined CuNCs and the presence of Cu in the EDS spectrum (Figure 4D) also confirmed the successful preparation of CuNCs. Compared with SEM, FE-SEM has a higher resolution. As shown in Figure 4E,F, interwoven fiber structures and cavities can be seen from FE-SEM images of CuNCs/ESM [56].

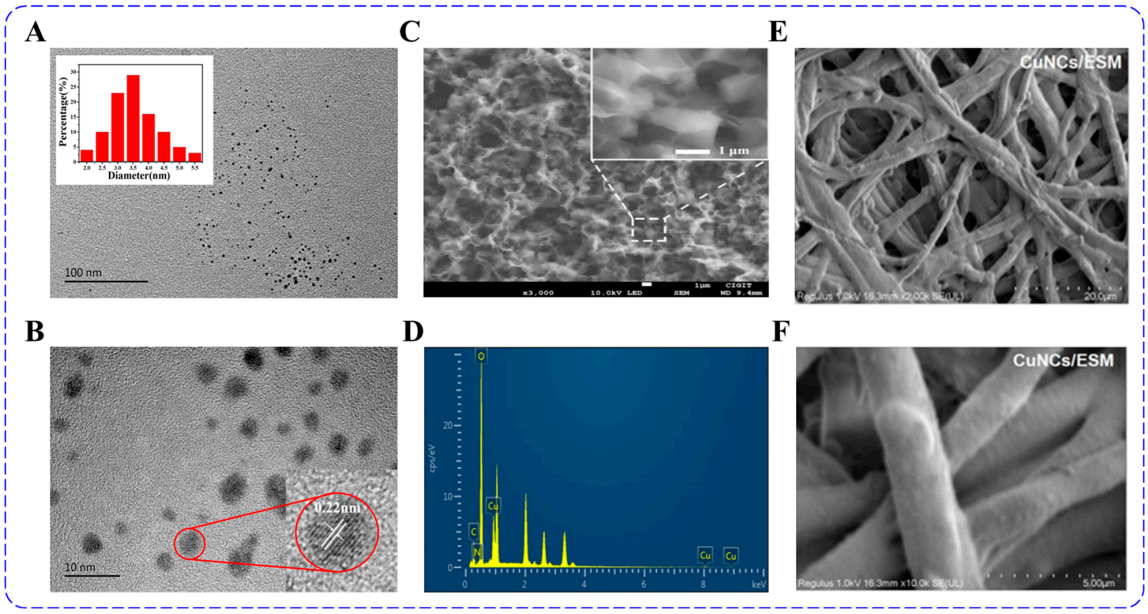


Figure 4. TEM (**A**) and HR-TEM (**B**) images of MMI-CuNCs [53], Copyrights from American Chemistry

Society, 2022. SEM image (**C**) and EDX spectrum (**D**) of CuNCs synthesized in poly-L-Cys film [58], Copyrights from American Chemistry Society, 2020. FE-SEM images of CuNCs/ESM at a magnification of 2000 (**E**) and 10,000 (**F**) respectively [56], Copyrights from Springer, 2019.

3.4. XPS and FT-IR

XPS, as a surface analysis tool, is typically used to study the element composition and valence of compounds to determine whether CuNCs are successfully generated [59]. Li et al. designed and synthesized BSA/DPA-CuNCs [60], and determined the presence of Cu (0) and Cu (I) in CuNCs by the XPS spectrum of Cu 2p (Figure 5A). Furthermore, a strong peak in the high-resolution XPS spectrum of S 2p (Figure 5B) revealed the presence of chemisorbed S on the surface of CuNCs, thus confirming the existence of Cu and S on the complex.

FT-IR is a tool for qualitative analysis of functional groups, which is usually used to judge the surface chemical environment and formation mechanism of CuNCs. Figure 5C shows the FT-IR spectra of pure D-Pen and D-Pen-CuNCs [61]. The tensile vibration of the S-H bond corresponding to the peak located at 2511 cm^{-1} in the FT-IR spectrum of pure D-Pen disappeared in D-Pen-CuNCs, indicating that the interaction between sulfhydryl group and Cu atoms formed Cu-S bonds covered on the surface of CuNCs. Simultaneously, combined with XPS data, it was verified that CuNCs were successfully synthesized with the D-Pen ligand as a stabilizer.

3.5. Others

Several characterization methods are also used to study the properties of CuNCs. Lin et al. prepared a bifunctional fluorescent nanohybrid based on CDs and CuNCs and characterized by XRD [62]. As shown in Figure 5D, there is a 43.7° diffraction peak in the XRD spectra of CuNCs and CDs-CuNCs, which corresponds to the Cu (111) crystal plane. TGA was used to study the thermal stability of solid CuNCs. As shown in Figure 5E, the MMI-CuNCs lose almost no weight when the temperature is lower than 260 °C [53]. When the temperature rises above 700 °C, the mass loss is 60.5%, indicating that the thermal stability of solid MMI-CuNC is good. In addition, ICP-AES is usually used to explore the content of Cu in CuNCs. In the work of Li et al. [56], it was mentioned that the content of Cu in Cu NC/ESM was 1.5% determined by ICP-AES. Similarly, EDX can also be used to analyze the elements and content of the sample. Luo et al. designed rod-like Ag CuNCs [63]. As shown in Figure 5F. EDX spectrum shows that the atomic percentages of Ag and Cu in the cluster are 63% and 37% respectively, consistent with the expected values [64].

3.6. Factors Affecting the Fluorescence of Copper Nanoclusters

The factors affecting the fluorescence of CuNCs include core size, pH, reactants, incubation time of reaction, storage method, and solvent. The size of CuNCs is affected by the amount of reducing agent, dispersant, temperature, and surfactant [65,66]. It was found that the fluorescence of CuNCs was different under different pH conditions. Sarathi Kundu et al. studied the pH response of CuNCs stabilized with lysosomes and found that the intensity of fluorescence emission increased with the decrease of solution pH [67]. The protein structure changes with a higher solution pH and more exposure of NCs to the solvent leads to more collisions. Because of this special performance, this kind of CuNCs has certain research value in the field of pH sensing. Incubation time is also an important factor. Wang et al. investigated the effect of incubation time on fluorescence in the detection of dinotefuran (DNF) by sulfur-doped carbon quantum dots and copper nanoclusters (S-CQDs/CuNCs) [68]. The incubation time of standard DNF solution with S-CQD/CuNCs mixture was 7 min. The ratiometric fluorescence ratio increased gradually from 0 to 6 min. After 7 min, the incubation time and the ratio fluorescence ratio were in the equilibrium region. In addition, the solvent will have an effect on the fluorescence of the substance. Ning et al. prepared an atomically precise Cu_{10} alkyne cluster [69]. The Dichloromethane (DCM) solution of Cu_{10} was transformed into a Cu_{18} cluster with enhanced fluorescence

efficiency after being added with hexane. The solvent-induced the transformation of the structure from a parallelepiped to an hourglass structure.

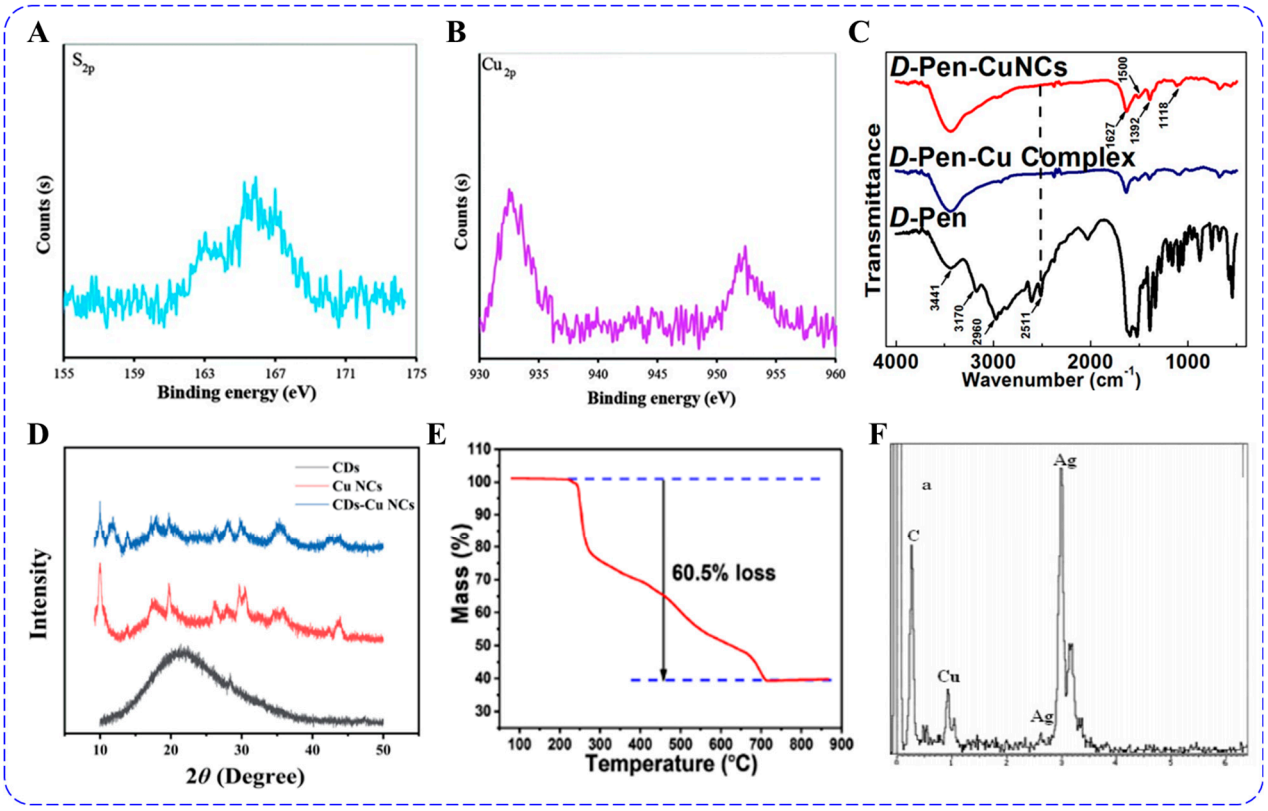


Figure 5. High-resolution XPS spectra of Cu 2p (**A**) and S 2p (**B**) of BSA/DPA-CuNCs [60], Copyrights from Royal Society Chemistry, 2016. (**C**) FT-IR spectra of D-Pen-CuNCs and other controls [61], Copyrights from Royal Society Chemistry, 2016. (**D**) XRD spectra of CDs-CuNCs and other controls [62], Copyrights from Royal Society Chemistry, 2021. (**E**) TGA curve of MMI-CuNCs [53], Copyrights from American Chemistry Society, 2022. (**F**) EDX spectrum of Ag-CuNCs [64], Copyrights from Elsevier, 2021.

4. Mechanism of Fluorescent Sensors

Fluorescent probes are commonly used to detect targeted ions or molecules. The interaction between fluorophores and target molecules leads to fluorescence enhancement or quenching. The possible mechanisms include static quenching, dynamic quenching, electron transfer (ET), inner filter effect (IFE), aggregation-induced quenching (AIQ), aggregation-induced enhancement (AIE), and forster resonance energy transfer (FRET). The following is a brief introduction to several mechanisms and their basis.

4.1. Aggregation-Induced Quenching

AIQ is one of the causes of fluorescence quenching, which can be well confirmed by TEM images and UV-vis absorption spectra. AIQ is the fluorescence quenching phenomenon of chromophores in a high concentration or aggregation state [70]. Shao et al. proposed the use of dithiothreitol (DTT) to make DTT-CuNCs for Co^{2+} detection [71]. The quenching mechanism is AIQ. In TEM characterization, a large amount of aggregation was observed in the presence of Co^{2+}. Meanwhile, in the UV-vis absorption spectra, the appearance of the new shoulder indicated that a non-luminescent polymer is formed. These two characteristics indicated that the quenching mechanism of the fluorescence sensor is AIQ. In another work, MMI-CuNCs were fabricated using 2-mercapto-1-methylimidazole (MMI) as a protective ligand to detect Ag^{+} [53]. In order to find out the cause of fluorescence quenching, a series of characterizations were performed. As the TEM image revealed

(Figure 6), Ag^+ and probes had obvious aggregation phenomena. Moreover, there was a new absorption peak appeared in UV-vis absorption spectra. Therefore, the quenching mechanism was also attributed to AIQ.

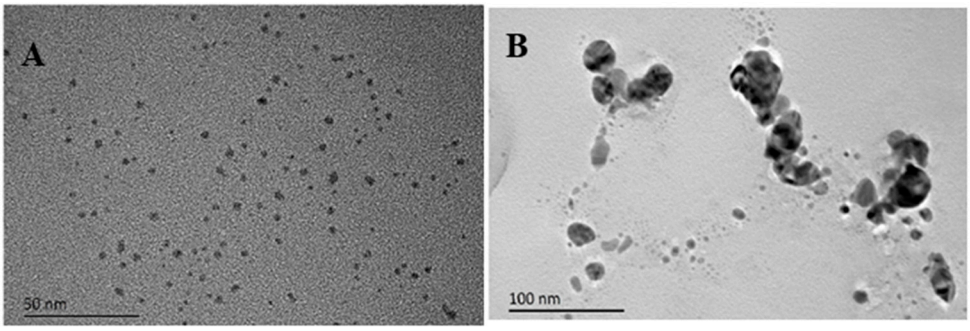


Figure 6. TEM images of MMI-CuNCs in the absence (**A**) and presence (**B**) of Ag^+ [53], Copyrights from American Chemistry Society, 2022.

4.2. Static Quenching & Dynamic Quenching

The quenching agent combines with fluorescent groups to produce non-luminescent fluorescent substances, which is static quenching. However, dynamic quenching is caused by the collision between the quencher and the fluorescence group. The absence of a significant change in the fluorescence lifetime of the fluorophore after the addition of the quenching agent indicates that static quenching occurs, whereas a significant change in the fluorescence lifetime confirms that the nature of quenching is dynamic [72]. In recent work, CuNCs can be used to detect iron ions, and tryptophan is selected as a reducing and protective agent in the synthesis process [45]. The detection mechanism of the probe is static quenching. In the presence and absence of irons ions, the lifetime of the probe did not change significantly. This proves that the cause of quenching is static quenching. So as to study the mechanism of quenching, Guo et al. used the Stern-Volmer equation to find the answer [73]. Stern-Volmer quenching constant increased with the increase in temperature, which proved that the quenching mechanism is dynamic quenching. At the same time, the reason for fluazinam quenching the fluorescence of samples was explained.

4.3. Inner Filter Effect

The fluorescence quenching induced by IFE is caused by the absorption of excitation or emission light from the fluorophore by the additive [74]. In a work by Shao et al., yeast powder was used as raw material to synthesize fluorescent probes, and its detection mechanism was IFE [55]. The fluorescence excitation spectra and emission spectra of yeast-carbon quantum dots (Y-CDs) overlapped with the UV-vis absorption spectra of the measured substance. In UV-vis absorption spectra, the absorption peak of Y-CDs disappeared with the increase of the dopamine (DA) concentration. At the same time, an absorption peak belonging to DA occurred. It was proved that the detection mechanism was IFE. In addition, Zhang et al. made FA-CuNCs probes with folic acid (FA) [75]. Its detection mechanism can also be attributed to the IFE. The UV-vis absorption spectra of the tested substance overlapped the excitation and emission spectra of FA-CuNCs to a great extent. The fluorescence lifetime did not change significantly, so it was concluded that the quenching mechanism was IFE [76].

4.4. Aggregation-Induced Enhancement

A substance that initially produces only weakly fluorescent or non-fluorescent, but has high emissivity when it is aggregate or solid and is defined as AIE [70]. Due to the aggregation of the molecule, its internal activity can be inhibited, thereby improving its luminescence efficiency. The fluorescence of tannin acid-CuNCs (TA-CuNCs) was enhanced by cetyltrimethyl ammonium bromide (CTAB) [77]. Because the electrostatic interaction

reduces the vibration and rotation of TA-CuNCs, the aggregation of molecules limits the intramolecular motion, and the fluorescence intensity of TA-CuNCs is enhanced due to the phenomenon known as an aggregation-induced enhancement (AIE).

4.5. Other Mechanisms

Shao et al. used different reducing agents to synthesize CuNCs in a single-layer eggshell membrane(ESM) to form CuNCs@ESM [56]. The CuNCs@ESM showed a fluorescence quenching reaction to Hg^{2+}. Hg^{2+} and functional groups formed complexes through coordination and electrostatic attraction, and the surface cap ligands and charge states of CuNCs changed. In this case, the fluorescence is quenched.

As a fluorescent probe for ions detection, CuNCs can detect heavy metal ions (HMIs) through fluorescence enhancement or quenching. Meanwhile, it can also achieve better visual monitoring with fluorescent strips or combined with smartphones, which can also be applied in a variety of complex environments. For the detection of HMIs, the possible detection mechanisms are only briefly outlined above (Figure 7).

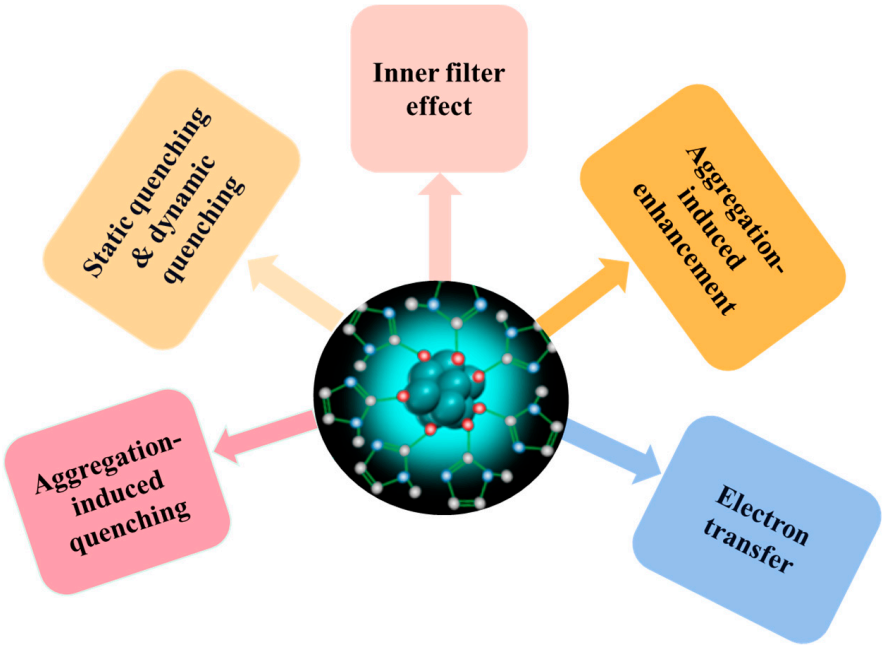


Figure 7. Common mechanisms of fluorescent sensors.

5. Copper Nanoclusters for Heavy Metal Ions Detection

HMIs can accumulate in the human body and cause poisoning. They can enter the biological chain from nature in many ways and are difficult to degrade in the body. HMIs can be detected by colorimetric methods, fluorescence methods, and point-of-care testing (POCT). POCT technology based on smartphone has the advantages of on-site diagnosis and portability. However, the technology relies on a wide variety of accessories that can be affected by environmental changes [78,79]. Colorimetric methods for color evaluation are an important problem, and another problem is the stability of color [79,80]. The fluorescence method is widely used in HMIs determination because of its advantages of simple operation, low cost, and high sensitivity [81]. In addition, the fluorescence sensor has the characteristics of strong specificity, fast detection speed, and high accuracy [34]. CuNCs are used as sensors to detect HMIs. The low-cost detection method brings convenience to the actual detection. The following are some of the works using CuNCs as fluorescence sensors to detect HMIs.

5.1. Silver Ion

Silver is used in cosmetics, industry, catalysts, and other fields. The discharge of waste liquid is widely used in industry and will also pollute water and soil [82]. Ag^+ has a great influence on human health. The accumulation of Ag^+ in the human body can cause cytotoxicity, body failure, and mitochondrial dysfunction [83]. Therefore, it is necessary to develop a simple and rapid silver ion detection method. The requirement of silver ion detection can be satisfied by using CuNCs as probes. Shao et al. made MMI-CuNCs as a probe to detect Ag^+ (Figure 8A) [53]. The protective agent was MMI, and the reducing agent was hydrazine hydrate. The detection limit was 6.7 nM, which could be applied to the detection of Ag^+ in human serum samples. Shao et al. also proposed to make a nanoprobe with dithiothreitol and eggshell membrane (ESM) [56]. Concurrently, they made a sensor to complete the detection of Ag^+. It caused fluorescence quenching in the presence of Ag^+ (Figure 8B). Zhang et al. synthesized CuNCs by sonochemistry using N-acetyl-L-cysteine (NAC) [84], which can be used for the selective detection of Ag^+ (Figure 8C). The limit of detection (LOD) was as low as 7.76×10^{-11} M. The detection mechanism was attributed to dynamic quenching. The addition of Ag^+ made the particles aggregate and the fluorescence lifetime of the NAC-CuNCs system decreased. Importantly, the synthesis process only takes 15 min, and the detection time is short in actual water samples. Glucose (Glc) was used as a reducing agent to prepare Glc-CuNPs [85], and the detection was completed by the fluorescence turn-off mechanism caused by the interaction between the probe and Ag^+. The fluorescence of Glc-CuNPs changed significantly with increasing Ag^+ concentration (Figure 8D). In addition, CuNCs/ZIF-8(72) was prepared using CuNCs, $Zn(NO_3)_2{\cdot}6H_2O$, 2-methylimidazole (2-MIM,72 mg) as raw materials [86]. Interestingly, CuNCs/ZIF-8(72) can also be used for Ag^+ detection by fluorescence turn-off mechanism (Figure 8E). The mechanism is the strong complexation between sulfhydryl in CuNCs/ZIF-8 (72) and Ag^+. The above-mentioned works (Table 1) prove the practicability and broad application prospect of CuNCs in Ag^+ detection. In the reports we investigated, the lowest detection limit of Ag^+ detected by CuNCs was 1.2 pM [87]. These works are performed by fluorescent turn-off mechanism to complete Ag^+ detection, which is applied to human serum or actual water samples. Using eggshell membrane as raw material to synthesize NCs has the advantages of green and low cost [88–90]. The synthesis of NCs by ultrasonic chemistry is also a useful way.

5.2. Mercury Ion

Major sources of mercury include fossil fuel burning and mineral industry production. Mercury does not degrade naturally and enters the human body through the biological chain causing serious effects [91]. Mercury can accumulate in various forms in living organisms. Long-term exposure to mercury can cause neurological dysfunction and interferes with cell function [92]. Therefore, the detection of mercury levels is essential for environmental and biological health. One of our works details the synthesis of CuNCs@ESM in situ on eggshell membranes (Figure 9A). The reducing agents were $N_2H_4{\cdot}H_2O$, $NH_2OH{\cdot}HCl$, and Vitamin C, and a strip sensor was made to detect Hg^{2+} [93]. The fabrication of sensing bands makes it easier and more convenient to monitor ions in real-time. Vasimalai et al. synthesized TG-CuNCs using 1-thio-β-glucose as a ligand (Figure 9B) [94]. The detection limit of Hg^{2+} is 1.7 nM. At the same time, a smartphone-assisted paper kit was designed for on-site monitoring of Hg^{2+} in tap water, rivers, and ponds. Furthermore, CuNCs prepared with turmeric root extract as a template can be used as a fluorescence probe to detect Hg^{2+} (Figure 9C), and its quenching mechanism was AIQ [95]. At room temperature, the linear range was 0.0005–25 μM, and the detection limit is 0.12 nM. The analysis of tap water, river water, and canal water demonstrated that the method had good accuracy. Importantly, the biomass used to synthesize CuNCs comes from nature and is more environmentally friendly. Yang et al. made carbon dots-CuNCs (CDs-CuNCs) with dual-emission wavelengths [96]. In the presence of Hg^{2+}, the pink fluorescence changes to blue fluorescence. The addition of Hg^{2+} decreased the red fluorescence of CuNCs (Figure 9D). A simple and sensitive test

paper was developed for rapid detection and visualization. Zhang et al. used $AgNO_3$ and Cu $(NO_3)_2$ to construct silver/copper bimetallic nanoparticles (AgCu-BNPs) [97]. The addition of Hg^{2+} enabled the bimetallic probe to perform selective detection by colorimetric and fluorescence modes. The minimum concentration limits of colorimetric and fluorescence methods were 89 nM and 9 nM, respectively. The blue fluorescence of AgCu-BNPs was quenched by Hg^{2+}, and the system was accompanied by the visible color change (Figure 9E). The quenching mechanism was attributed to IFE, static quenching, and dynamic quenching. Dual-mode detection made the detection more simple and more reliable. The above reports are related to the detection of Hg^{2+} by CuNCs (Table 2). The probes were designed into strip sensor belts or combined with a smartphone [98], which was more suitable for detection in complex environments. The NCs prepared by turmeric root extract extends the application value of biomass materials. CDs-CuNCs are nanocomposites with dual emission wavelengths assembled by simple electrostatic discharge. The synthesis of double-emission materials by green materials and chemical means is also worth studying. In a survey of the latest work [99,100], gold nanoparticles were combined with a resolution matrix-assisted laser desorption ionization time-of-flight mass spectrometer (MALDI-TOF MS) for measurement [99]. The detection limit of Hg^{2+} was 0.19 pmol/μL.

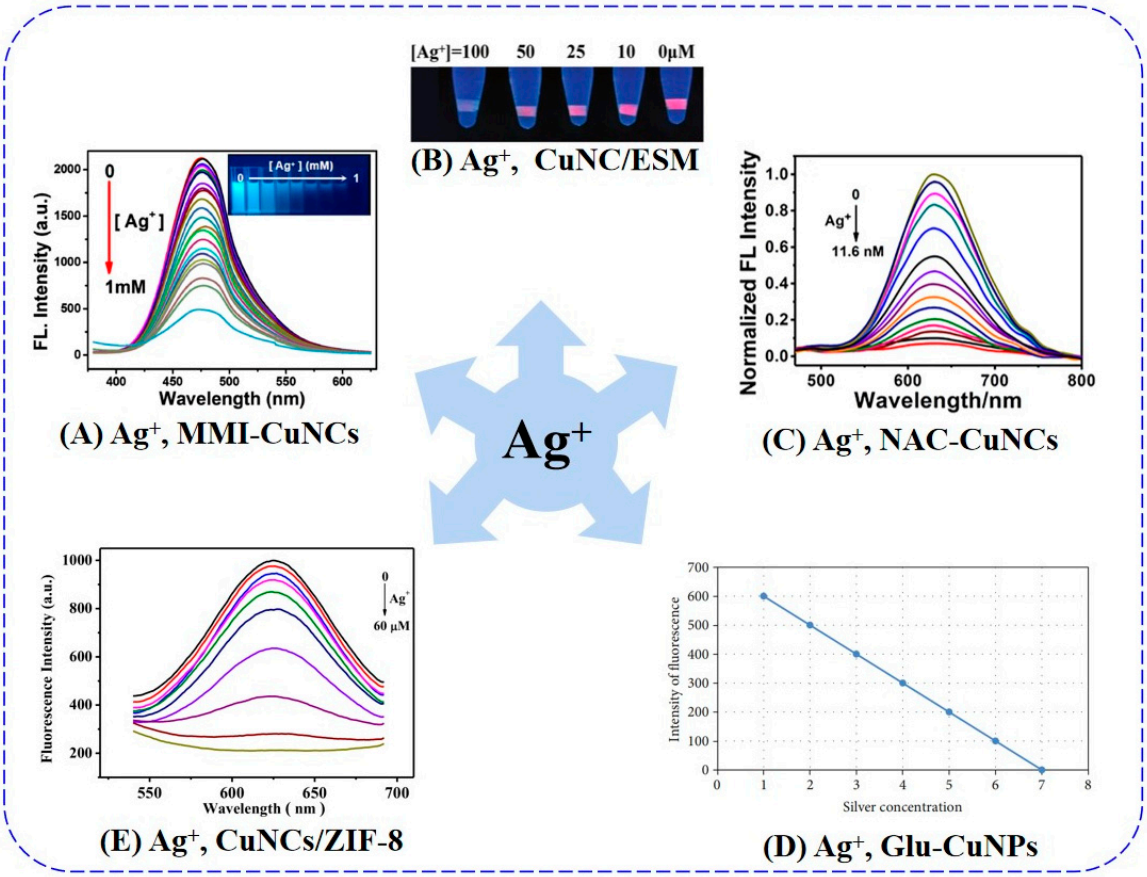


Figure 8. CuNCs for Ag^+ detection. (**A**) Fluorescence emission spectra in the presence of Ag^+ using MMI-CuNCs as a probe. Inset: the photo of MMI-CuNCs under a UV lamp [53], Copyrights from American Chemistry Society, 2022. (**B**) The photo of CuNC/ESM in the presence of Ag^+ from 0 to 100 μM under a UV lamp [56], Copyrights from Springer, 2019. Fluorescence spectra of different concentrations of Ag^+ injected into (**C**) NAC-CuNCs [84], Copyrights from Elsevier, 2022. and (**E**) CuNCs/ZIF-8 [86], Copyrights from Elsevier, 2022. (**D**) The relationship between Glu-CuNPs absorption spectra and Ag^+ concentration [85], Copyrights from Hindawi, 2022.

Table 1. Report on detection of Ag^+ by CuNCs.

Type of CuNCs	$\lambda_{ex}/\lambda_{em}$ (nm)	Read Out	Sensing Mechanism	Reaction Time	Limit of Detection	Published Time	Reference Value	Ref.
MMI-CuNCs	322/476	Turn-off	AIQ, Static quenching	30 min	6.7 nM	2022		[53]
CuNC/ESM	360/623	Turn-off	high-affinity metallophilic interactions	—	—	2019	1.2 pM 2021 [87]	[56]
NAC-CuNCs	340/630	Turn-off	dynamic quenching	2 min	7.76×10^{-11} M	2022		[84]
Glc-CuNPs	472/542	Turn-off	AIQ	30 min	—	2022		[85]
CuNCs/ZIF-8	360/627	Turn-off	the formation of Ag-S bonds	3 min	0.33 μM	2022		[86]

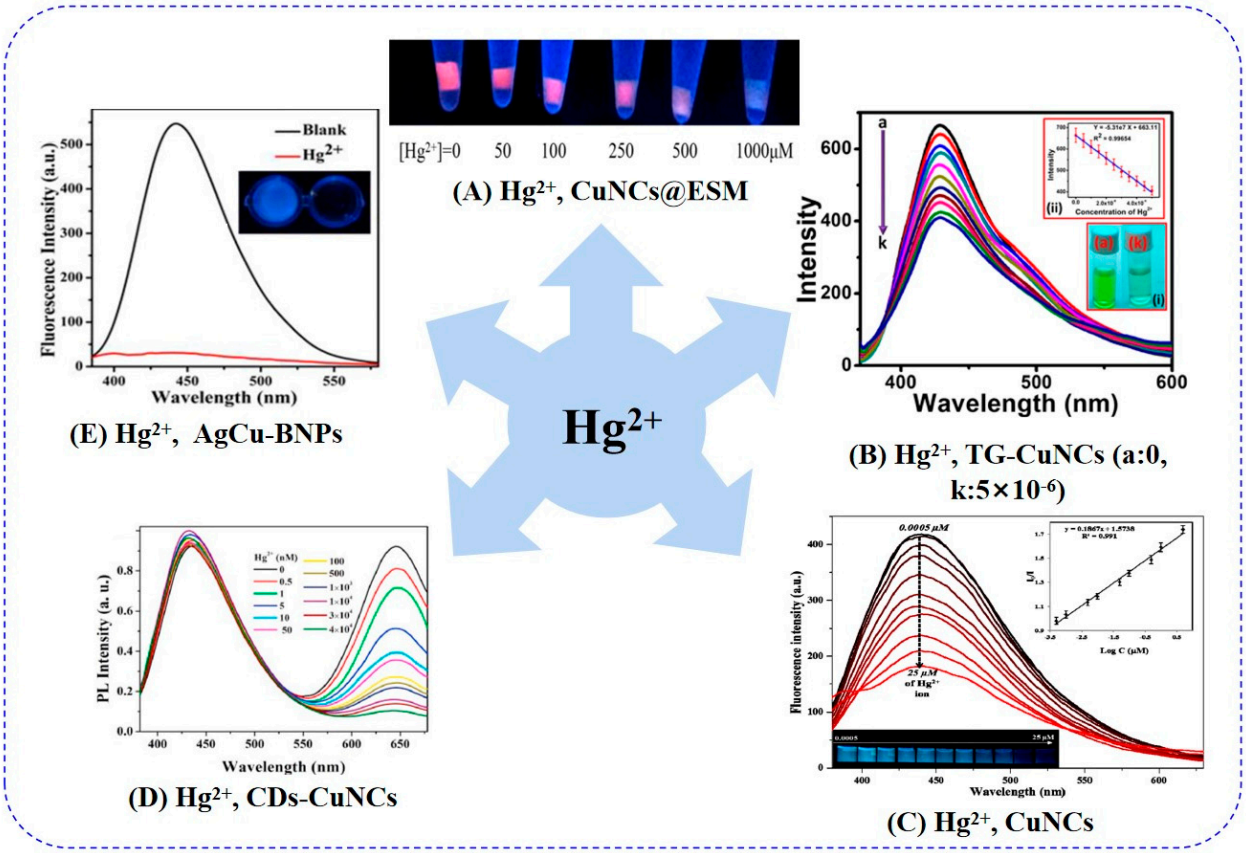


Figure 9. CuNCs for Hg^{2+} detection. (**A**) The photo of CuNCs@ESM in the presence of Hg^{2+} from 0 to 1000 μM under a UV lamp [93], Copyrights from MDPI, 2018. Fluorescence spectra of different concentrations of Hg^{2+} injected into (**B**) TG-CuNCs [94], Copyrights from Elsevier, 2020. (**C**) CuNCs [95], Copyrights from Royal Society Chemistry, 2018; and (**D**) CDs-CuNCs [96], Copyrights from Elsevier, 2021. (**E**) Fluorescence spectra of AgCu-BNPs and with Hg^{2+} [97], Copyrights from Elsevier, 2021.

Table 2. Report on detection of Hg^{2+} by CuNCs.

Type of CuNCs	λex/λem (nm)	Read Out	Sensing Mechanism	Reaction Time	Limit of Detection	Published Time	Reference Value	Ref.
CuNCs@ESM	—	Turn-off	high-affinity metallophilic interactions	1 h (Hg^{2+}: 500 μM)	—	2018	0.19 pmol/μL 2023 [99]	[93]
TG-CuNCs	350/430	Turn-off	static and dynamic quenching	3 min	1.7 nM	2020		[94]
CuNCs	365/440	Turn-off	AIQ	22 min	0.12 nM	2018		[95]
CD-CuNCs	dual-emission	—	strong affinity	—	0.31 nM	2021		[96]
AgCu-BNPs	350/442	Turn-off	IFE, static and dynamic quenching	—	9 nM	2021		[97]

5.3. Iron Ions

The presence of Fe^{3+} allows many physiological processes to proceed normally. However, too much Fe^{3+} can lead to serious diseases such as cancer, Parkinson's, and Alzheimer's [101]. Among the methods for detecting iron ions (Table 3), the fluorescence method is a good choice for sensor manufacturing because of its high sensitivity [102]. Cao et al. recently assembled BSA-CuNCs @ $[Ru(bpy)_3]^{2+}$ from bovine serum albumin (BSA)-CuNCs and $[Ru(bpy)_3]^{2+}$ to detect Fe^{3+} in tap water and spirits [103]. BSA-CuNCs @ $[Ru(bpy)_3]^{2+}$ show two distinct emission peaks. $[Ru(bpy)_3]^{2+}$ did not respond to Fe^{3+}, and fluorescence quenching occurred in BSA-CuNCs. Additionally, a POCT platform based on a smartphone was designed for the actual detection of Fe^{3+} (Figure 10A). Moreover, Cysteamine functionalized nanoconjugate materials (CA-CuNCs) can be used to determine Fe^{3+} in human urine (Figure 10B) [104]. The detection mechanism was based on electron transfer and AIQ. Importantly, the stratified test strips were designed, and the brightness changed greatly before and after adding Fe^{3+}. Ai et al. used duplex oligonucleotide (ds-DNA) as a template to prepare copper nanomaterials (dsDNA-CuNCs), which showed its applicability as a Fe^{3+} sensor; fluorescence quenching was caused by the aggregation of nanomaterial particles [105]. The detection limit was 5 μM when Fe^{3+} concentration was 5–100 μM (Figure 10C). Hemmateenejad et al. synthesized Penicillamine-capped bimetallic Gold-Copper NCs (PA-AuCu-bi-MNCs). The milky water solution demonstrated orange fluorescence under a UV lamp [101]. It can be used for simple quantitative detection of Fe^{3+} (Figure 10D), utilizing the detection mechanism of IFE. It was important that the detection process is free from Fe^{2+} interference. In the literature investigated, the minimum detection limit of Fe^{3+} detected by CuNCs was 10 nM. CuNCs made of bovine serum albumin (BSA) by Debanjan Guin et al. could be applied to the detection of ions in wastewater and human serum samples [106].

Table 3. The recent report on the detection of Fe^{3+} by CuNCs.

Type of CuNCs	λex/λem (nm)	Read Out	Sensing Mechanism	Reaction Time	Limit of Detection	Published Time	Reference Value	Ref.
BSA-CuNCs@ $[Ru(bpy)_3]^{2+}$	Dual-emission	—	AIQ	3 min	0.086 μM	2022	10 nM	[103]
CA-CuNCs	385/467	Turn-off	electron transfer, AIQ	—	423 nM	2020	2022 [106]	[104]
dsDNA-CuNCs	312/400	Turn-off	AIQ	1 h	5 μM	2020		[105]
PA-AuCu-bi-MNCs	275/605	Turn-off	IFE	5 min	0.1 μM	2019		[101]

5.4. Cobalt Ion

Cobalt is an essential trace element, but ingesting high concentrations or prolonged exposure can still cause illness, including contact dermatitis, pneumonia, allergic asthma, and lung cancer [107]. Shao et al. used dithiothreitol (DTT) to make DTT-CuNCs to detect Co^{2+} (Figure 11A), and the detection mechanism was AIQ [71]. The DTT-CuNCs probe was fixed to the filter paper and designed as a visual paper sensor with the help of a mobile phone, which had good applications in water samples and other environments. Ling et al. found that GSH-AuNCs made from glutathione (GSH) can selectively detect Co^{2+} [108]. The detection process was accomplished by adjusting the pH. When the pH was 6, the presence of Co^{2+} can effectively quench the fluorescence of NCs, and the quenching mechanism was static quenching. He et al. used lysozyme (Lys) and hydroxylamine hydrochloride ($NH_2OH{\cdot}HCl$) as raw materials to make Lys-CuNCs, which showed strong yellow fluorescence under an ultraviolet lamp [109]. It can be used for sensitive and selective detection of Co^{2+} in an aqueous solution with a detection limit of 2.4 nM. Above are related reports on the application of MNCs in Co^{2+} detection (Table 4), which needs to be further developed. In recent work, Tong et al. used silicon nanoparticles/gold nanoparticles complex as a fluorescent probe to detect Co^{2+}, and the detection limit was as low as 60 nM [110]. The detection of ions by GSH-AuNCs was completed by adjusting pH,

indicating that pH value would have an impact on the detection process and was also an important factor affecting the fluorescence of substances.

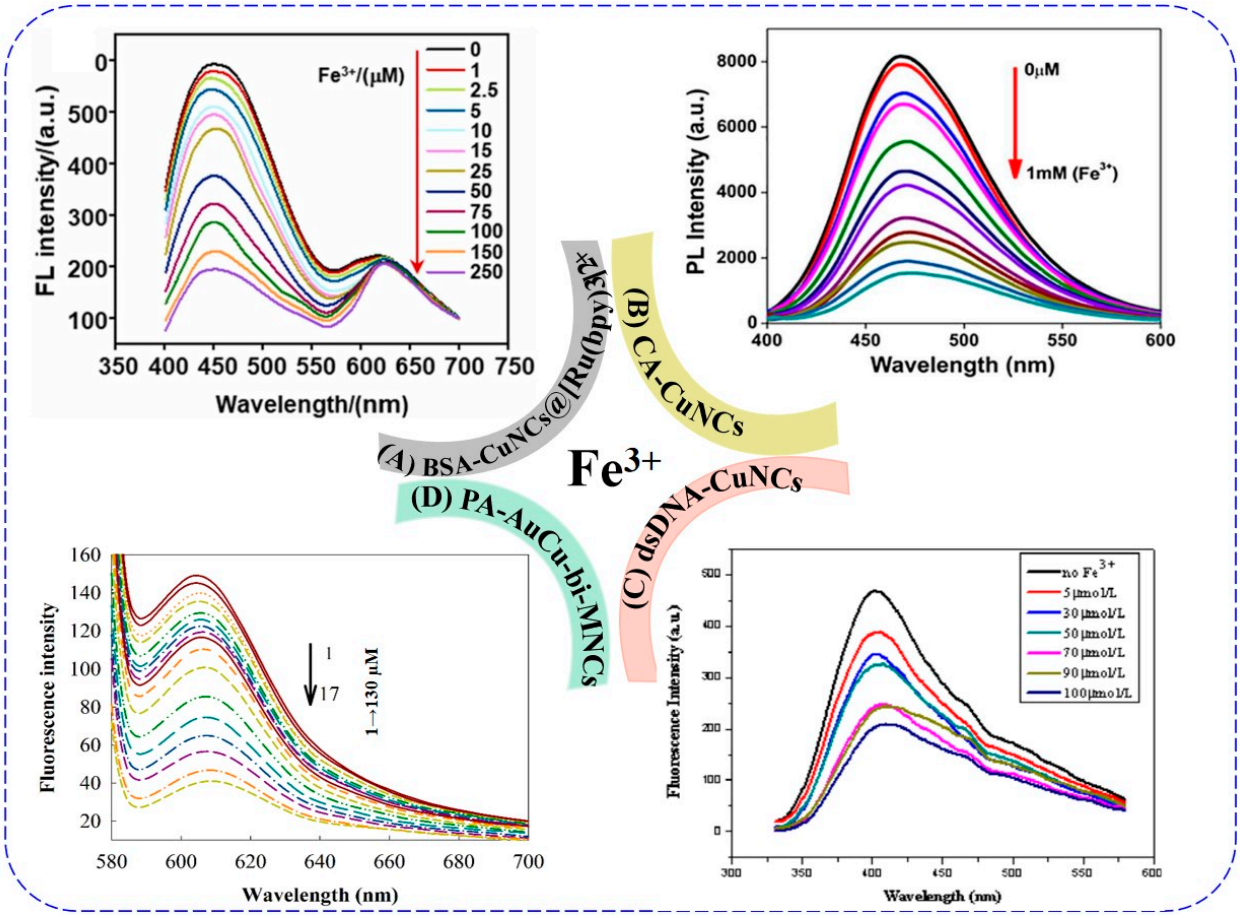


Figure 10. CuNCs for Fe^{3+} detection. Fluorescence spectra of different concentrations of Fe^{3+} injected into (**A**) BSA-CuNCs @ $[Ru(bpy)_3]^{2+}$ [103], Copyrights from Elsevier, 2022; (**B**) CA-CuNCs [104], Copyrights from Elsevier, 2020; (**C**) dsDNA-CuNCs [105], Copyrights from IOP Publishing, 2020; and (**D**) PA-AuCu-bi-MNCs [101], Copyrights from Elsevier, 2019.

5.5. Other Ions

CuNCs have also been synthesized for the detection of other HMIs. For instance, Cr (VI) contamination is highly associated with atopic dermatitis, carcinogenesis, and mutations in animals and humans. Hu et al. synthesized CuNCs using thiosalicylic acid (TA) and cysteamine (CysA) as ligands [111]. Because the IFE effect quenches the fluorescence of CuNCs, a fluorescence sensor was designed to detect Cr (VI) (Figure 11B). In addition, He et al. synthesized water-soluble CuNCs stabilized by DNA single base thymine and performed selective detection of Mn^{2+} based on AIE (Figure 11C) [112]. Cadmium is highly toxic, known as a carcinogen, and in large quantities can damage the liver, bones, and kidneys. Furthermore, high levels of cadmium have been linked to diabetes, cancer, and heart disease [114]. Liu et al. used the glutathione@carbon dots (GSH@CDs) as a template for the synthesis of GSH@CDs-CuNCs, which can be used to detect Cd^{2+} (Figure 11D). The linear range of Cd^{2+} was 0~20 $\mu mol \cdot L^{-1}$, and the limit of detection was 0.6 $\mu mol \cdot L^{-1}$ [113].

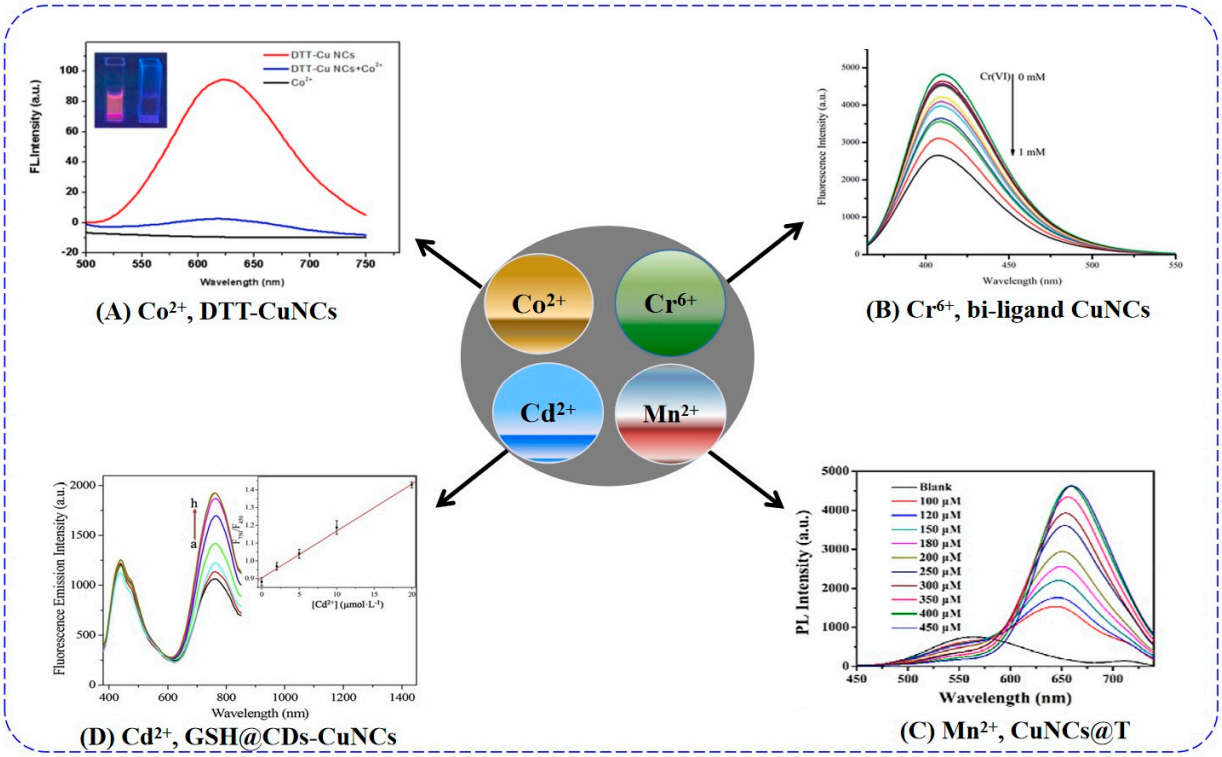


Figure 11. (**A**) Fluorescence spectra of DTT-CuNCs and with Co^{2+} [71], Copyrights from Elsevier, 2021. Different concentrations of HMIs were added to (**B**) bi-ligand CuNCs [111], Copyrights from Royal Society Chemistry, 2019; (**C**) CuNCs@T [112], Copyrights from Royal Society Chemistry, 2017; and (**D**) GSH@CDs-CuNCs [113], Copyrights from Elsevier, 2020.

Those listed above are just a few examples of CuNCs detecting HMIs. (Table 4) These works further elucidate the possibility of CuNCs for ions detection and provide a new approach for the detection of HMIs.

Table 4. The list reported HMIs detection via CuNCs.

Metal Ions	Type of CuNCs	$\lambda_{ex}/\lambda_{em}$ (nm)	Read Out	Sensing Mechanism	Reaction Time	Limit of Detection	Published Time	Reference Value	Ref.
Co^{2+}	DTT-CuNCs	382/627	Turn-off	AIQ	30 min	25 nM	2021	60 nM	[71]
	GSH-AuNCs	412/500	Turn-off	Static quenching	15 min	0.124 μM (Co^{2+}: 2.0–50.0 μM)	2021	2022 [110]	[108]
	Lys-CuNCs	334/596	Turn-off	—	—	2.4 nM	2018		[109]
Cr^{6+}	bi-ligand CuNCs	330/411 (Cu NC-2 [a])	Turn-off	IFE	—	0.03 mM	—	—	[111]
Mn^{2+}	CuNCs@T [b]	354/561	Turn-on	AIE	40 min	10 μM	—	—	[112]
Cd^{2+}	GSH@CDs-CuNCs	dual-emission	—	AIE (750 nm)	15 min	0.6 μmol·L^{-1}	—	—	[113]

Cu NC-2 [a]: TA-to-CysA molar ratio of 1:1, T [b]: Rich-thymine.

5.6. Selectivity Difference of CuNCs in Detecting HMIs

Heavy metal ions have a great influence on organisms and the environment, so fluorescence sensing for HMIs detection is of great significance. There were significant differences in CuNCs detection among different HMIs. For example, different fluorescence responses, and different fluorescence intensities. Huang et al. prepared CuNCs using bovine serum albumin (BSA) and thiosalicylic acid (TSA) as protective ligands [115]. The fluorescence changes produced by TSA/BSA-CuNCs interacting with various metal ions (incubated in sodium phosphate buffer) were observed. Only Cr^{6+} showed significant fluorescence quenching on TSA/BSA-CuNCs due to the IFE. Cr^{6+} provides sufficient oxidative etching of copper ions/atoms. Olga Garcia et al. designed a sensor for the detection of Hg^{2+} by taking advantage of the differences in the detection of metal ions

by CuNCs [116]. CuNCs were tested on various metal ions under the same conditions, and the fluorescence attenuation was nearly 50% only in the presence of Hg^{2+}, and the effect was small in the presence of other ions. CuNCs were incubated with a series of Hg^{2+} concentrations, and the hydrodynamic size was gradually increased. No changes in the hydrodynamic size were detected in the presence of Cd^{2+}. This kind of CuNCs can be used as selective probes to detect Hg^{2+} in the presence of other ions. It has also been mentioned that the CDs-CuNCs synthesized by Yang et al. have dual emission wavelengths [96]. The addition of Hg^{2+} reduced the red emission of CuNCs, while the blue emission of CDs remained stable. As a result, the fluorescent color changes from pink to blue.

6. Outlook and Challenges

To summate, we have described the synthesis, characterization, and application of CuNCs in HMIs detection, highlighting the attractive merits of CuNCs as a new material. However, researchers have studied Au, Ag, and other noble metal NCs in depth, while the research on CuNCs is relatively simple. Therefore, there are still many new challenges for CuNCs. For example, compared with semiconductor quantum dots, CuNCs have relatively low fluorescence quantum yield and weak luminescence. Thus, how to prepare strong luminescence and high quantum yield is one of the many challenges CuNCs faces. Additionally, CuNCs are easily oxidized and unstable, which makes them challenging in synthesis and preservation. Finally, CuNCs are also required to possess good stability and other excellent properties in fluorescence analysis and other applications. Therefore, the problem to obtain monodisperse and stable water-soluble CuNCs remains unsolved. We believe that ultra-sensitive and more portable analytical detection applications based on CuNCs will be developed in the future.

7. Conclusions

The development and diversification of nanomaterials have promoted the development of HMI detection. In this review, we discuss the detection of HMIs by CuNCs. From the different synthesis strategies of CuNCs and related characterization to the detection mechanism of HMIs by CuNCs, relevant reports are also listed. The difficulty of synthesis lies in achieving the production of CuNCs with good stability. After adding different HMIs, fluorescence enhancement or quenching occurs under different mechanisms. Compared with other HMIs detection methods, the fluorescence method can meet the requirements for real-time detection in complex environments, with better selectivity and sensitivity. Although this method has made great progress, it still has the possibility of development in synthesis, purification, and application.

Author Contributions: Conceptualization, S.L. and C.S.; writing—original draft preparation, L.Y. and M.L.; writing—review and editing, S.L.; visualization, revision, formal analysis, data curation, revision, M.H.; project administration, S.L.; funding acquisition, S.L. and C.S. All authors have read and agreed to the published version of the manuscript.

Funding: This work was financially supported by Natural Science Foundation of Chongqing (Grant No. CSTB2022NSCQ-BHX0035), Special Research Assistant Program of Chinese Academy of Science, Research and development of novel fluorescent nanomaterials (No. 22100191), Natural Science Foundation of Anhui Provincial Department of Education (No. KJ2019A0598), Natural Science Foundation of Anhui Province (No. 1708085QB44) and Excellent Young Talents Fund Program of Higher Education Institutions of Anhui Province (No. gxyq2019168).

Institutional Review Board Statement: Not applicable.

Informed Consent Statement: Not applicable.

Data Availability Statement: Data Availability Statements are available in section "MDPI Research Data Policies".

Conflicts of Interest: The authors declare no conflict of interest.

References

1. Gumpu, M.B.; Sethuraman, S.; Krishnan, U.M.; Rayappan, J.B.B. A review on detection of heavy metal ions in water—An electrochemical approach. *Sensor Actuators B Chem.* **2015**, *213*, 515–533. [CrossRef]
2. Bansod, B.; Kumar, T.; Thakur, R.; Rana, S.; Singh, I. A review on various electrochemical techniques for heavy metal ions detection with different sensing platforms. *Biosens. Bioelectron.* **2017**, *94*, 443–455. [CrossRef]
3. Nayan Kumar, H.N.; Nagaraju, D.H.; Yhobu, Z.; Shivakumar, P.; Manjunatha Kumara, K.S.; Budagumpi, S.; Praveen, B.M. Recent advances in on-site monitoring of heavy metal ions in the environment. *Microchem. J.* **2022**, *182*, 107894. [CrossRef]
4. Fu, F.; Wang, Q. Removal of heavy metal ions from wastewaters: A review. *J. Environ. Manag.* **2011**, *92*, 407–418. [CrossRef]
5. Soliman, N.K.; Moustafa, A.F. Industrial solid waste for heavy metals adsorption features and challenges; a review. *J. Mater. Res. Technol.* **2020**, *9*, 10235–10253. [CrossRef]
6. Lu, S.; Hummel, M.; Chen, K.; Zhou, Y.; Kang, S.; Gu, Z. Synthesis of Au@ZIF-8 nanocomposites for enhanced electrochemical detection of dopamine. *Electrochem. Commun.* **2020**, *114*, 106715. [CrossRef]
7. Nie, M.; Lu, S.; Lei, D.; Yang, C.; Zhao, Z. Rapid Synthesis of ZIF-8 Nanocrystals for Electrochemical Detection of Dopamine. *J. Electrochem. Soc.* **2017**, *164*, H952–H957. [CrossRef]
8. Rotake, D.; Darji, A.D. Heavy Metal Ion Detection in Water using MEMS Based Sensor. *Mater. Today Proc.* **2018**, *5*, 1530–1536. [CrossRef]
9. Xu, N.; Jin, S.; Wang, L. Metal nanoparticles-based nanoplatforms for colorimetric sensing: A review. *Rev. Anal. Chem.* **2021**, *40*, 1–11. [CrossRef]
10. Lu, S.; Hummel, M.; Kang, S.; Gu, Z. Selective Voltammetric Determination of Nitrite Using Cobalt Phthalocyanine Modified on Multiwalled Carbon Nanotubes. *J. Electrochem. Soc.* **2020**, *167*, 7982. [CrossRef]
11. Lu, S.; Jia, H.; Hummel, M.; Wu, Y.; Wang, K.; Qi, X.; Gu, Z. Two-dimensional conductive phthalocyanine-based metal-organic frameworks for electrochemical nitrite sensing. *RSC Adv.* **2021**, *11*, 4472–4477. [CrossRef] [PubMed]
12. Lu, S.; Yang, C.; Nie, M. Hydrothermal synthesized urchin-like nickel-cobalt carbonate hollow spheres for sensitive amperometric detection of nitrite. *J. Alloy. Compd.* **2017**, *708*, 780–786. [CrossRef]
13. Zhu, Y.; Lu, S.; Gowri Manohari, A.; Dong, X.; Chen, F.; Xu, W.; Shi, Z.; Xu, C. Polydopamine interconnected graphene quantum dots and gold nanoparticles for enzymeless H_2O_2 detection. *J. Electroanal. Chem.* **2017**, *796*, 75–81. [CrossRef]
14. Dong, X.; Xu, C.; Lu, S.; Wang, R.; Shi, Z.; Cui, Q.; You, T. ZIF-8 Coupling with Reduced Graphene Oxide to Enhance the Electrochemical Sensing of Dopamine. *J. Electrochem. Soc.* **2021**, *168*, 116517. [CrossRef]
15. Lu, S.; Hummel, M.; Gu, Z.; Gu, Y.; Cen, Z.; Wei, L.; Zhou, Y.; Zhang, C.; Yang, C. Trash to treasure: A novel chemical route to synthesis of NiO/C for hydrogen production. *Int. J. Hydrog. Energy* **2019**, *44*, 16144–16153. [CrossRef]
16. Wan, N.; Wang, T.; Tan, X.-y.; Lu, S.; Zhou, L.-l.; Huang, J.-q.; Pan, W.; Yang, Y.-m.; Shao, Z.-y. Microstructure Related Synergic Sensoring Mechanism in Graphene Oxide Humidity Sensor. *J. Phys. Chem. C* **2018**, *122*, 830–838. [CrossRef]
17. Lu, S.; Hummel, M.; Wang, X.; He, W.; Pathak, R.; Dong, X.; Jia, H.; Gu, Z. Communication—In Situ Electrodeposition of Nickel Phosphide on Ni Foam for Non-Enzymatic Detection of Nitrite. *J. Electrochem. Soc.* **2020**, *167*, 146517. [CrossRef]
18. Lu, S.; Wang, Y.; Xiang, H.; Lei, H.; Xu, B.B.; Xing, L.; Yu, E.H.; Liu, T.X. Mass transfer effect to electrochemical reduction of CO_2: Electrode, electrocatalyst and electrolyte. *J. Energy Storage* **2022**, *52*, 104764. [CrossRef]
19. Waheed, A.; Mansha, M.; Ullah, N. Nanomaterials-based electrochemical detection of heavy metals in water: Current status, challenges and future direction. *Trac Trend. Anal. Chem.* **2018**, *105*, 37–51. [CrossRef]
20. Wang, Y.; Lei, H.; Lu, S.; Yang, Z.; Xu, B.B.; Xing, L.; Liu, T.X. Cu_2O nano-flowers/graphene enabled scaffolding structure catalyst layer for enhanced CO_2 electrochemical reduction. *Appl. Catal. B* **2022**, *305*, 121022. [CrossRef]
21. Brzechwa-Chodzyńska, A.; Drożdż, W.; Harrowfield, J.; Stefankiewicz, A.R. Fluorescent sensors: A bright future for cages. *Coord. Chem. Rev.* **2021**, *434*, 213820. [CrossRef]
22. Qin, D.-D.; Tang, Y.; Ma, G.; Qin, L.; Tao, C.-L.; Zhang, X.; Tang, Z. Molecular metal nanoclusters for ORR, HER and OER: Achievements, opportunities and challenges. *Int. J. Hydrogen. Energ.* **2021**, *46*, 25771–25781. [CrossRef]
23. Xiao, Y.; Wu, Z.; Yao, Q.; Xie, J. Luminescent metal nanoclusters: Biosensing strategies and bioimaging applications. *Agg* **2021**, *2*, 114–132. [CrossRef]
24. Zhao, Z.; Li, Y. Developing fluorescent copper nanoclusters: Synthesis, properties, and applications. *Colloids Surf. B* **2020**, *195*, 111244. [CrossRef]
25. Guo, Y.; Cao, F.; Lei, X.; Mang, L.; Cheng, S.; Song, J. Fluorescent copper nanoparticles: Recent advances in synthesis and applications for sensing metal ions. *Nanoscale* **2016**, *8*, 4852–4863. [CrossRef]
26. Ou, G.; Zhao, J.; Chen, P.; Xiong, C.; Dong, F.; Li, B.; Feng, X. Fabrication and application of noble metal nanoclusters as optical sensors for toxic metal ions. *Anal. Bioanal. Chem.* **2018**, *410*, 2485–2498. [CrossRef] [PubMed]
27. Maity, S.; Bain, D.; Patra, A. An overview on the current understanding of the photophysical properties of metal nanoclusters and their potential applications. *Nanoscale* **2019**, *11*, 22685–22723. [CrossRef] [PubMed]
28. Yang, J.; Peng, Y.; Li, S.; Mu, J.; Huang, Z.; Ma, J.; Shi, Z.; Jia, Q. Metal nanocluster-based hybrid nanomaterials: Fabrication and application. *Coord. Chem. Rev.* **2022**, *456*, 214391. [CrossRef]
29. Borse, S.; Jha, S.; Murthy, Z.V.P.; Kailasa, S.K. Sustainable chemistry approach for the preparation of bluish green emissive copper nanoclusters from Justicia adhatoda leaves extract: A facile analytical approach for the sensing of myoglobin and l-thyroxine. *New J. Chem.* **2022**, *46*, 15919–15928. [CrossRef]

30. An, Y.; Ren, Y.; Bick, M.; Dudek, A.; Hong-Wang Waworuntu, E.; Tang, J.; Chen, J.; Chang, B. Highly fluorescent copper nanoclusters for sensing and bioimaging. *Biosens. Bioelectron.* **2020**, *154*, 112078. [CrossRef] [PubMed]
31. Lin, Y.-S.; Lin, Y.-F.; Nain, A.; Huang, Y.-F.; Chang, H.-T. A critical review of copper nanoclusters for monitoring of water quality. *Sens. Actuators Rep.* **2021**, *3*, 10026. [CrossRef]
32. Bigdeli, A.; Ghasemi, F.; Abbasi-Moayed, S.; Shahrajabian, M.; Fahimi-Kashani, N.; Jafarinejad, S.; Farahmand Nejad, M.A.; Hormozi-Nezhad, M.R. Ratiometric fluorescent nanoprobes for visual detection: Design principles and recent advances—A review. *Anal. Chim. Acta* **2019**, *1079*, 30–58. [CrossRef]
33. Dong, W.; Wang, R.; Gong, X.; Liang, W.; Dong, C. A far-red FRET fluorescent probe for ratiometric detection of l-cysteine based on carbon dots and N-acetyl-l-cysteine-capped gold nanoparticles. *Spectrochim. Acta A Mol. Biomol. Spectrosc.* **2019**, *213*, 90–96. [CrossRef] [PubMed]
34. Shin, Y.-H.; Teresa Gutierrez-Wing, M.; Choi, J.-W. Review—Recent Progress in Portable Fluorescence Sensors. *J. Electrochem. Soc.* **2021**, *168*, 017502. [CrossRef]
35. Baghdasaryan, A.; Burgi, T. Copper nanoclusters: Designed synthesis, structural diversity, and multiplatform applications. *Nanoscale* **2021**, *13*, 6283–6340. [CrossRef]
36. Babu Busi, K.; Palanivel, M.; Kanta Ghosh, K.; Basu Ball, W.; Gulyas, B.; Padmanabhan, P.; Chakrabortty, S. The Multifarious Applications of Copper Nanoclusters in Biosensing and Bioimaging and Their Translational Role in Early Disease Detection. *Nanomaterials* **2022**, *12*, 301. [CrossRef]
37. Lu, Y.; Wei, W.; Chen, W. Copper nanoclusters: Synthesis, characterization and properties. *Chinese Sci. Bull.* **2012**, *57*, 41–47. [CrossRef]
38. Deng, H.H.; Li, K.L.; Zhuang, Q.Q.; Peng, H.P.; Zhuang, Q.Q.; Liu, A.L.; Xia, X.H.; Chen, W. An ammonia-based etchant for attaining copper nanoclusters with green fluorescence emission. *Nanoscale* **2018**, *10*, 6467–6473. [CrossRef]
39. Nerthigan, Y.; Sharma, A.K.; Pandey, S.; Wu, H.F. Cysteine capped copper/molybdenum bimetallic nanoclusters for fluorometric determination of methotrexate via the inner filter effect. *Mikrochim. Acta* **2019**, *186*, 130. [CrossRef]
40. Zhou, F.; Cui, X.; Shang, A.; Lian, J.; Yang, L.; Jin, Y.; Li, B. Fluorometric determination of the activity and inhibition of terminal deoxynucleotidyl transferase via in-situ formation of copper nanoclusters using enzymatically generated DNA as template. *Microchim. Acta* **2017**, *184*, 773–779. [CrossRef]
41. Jiao, M.; Li, Y.; Jia, Y.; Xu, L.; Xu, G.; Guo, Y.; Luo, X. Ligand-modulated aqueous synthesis of color-tunable copper nanoclusters for the photoluminescent assay of Hg(II). *Mikrochim. Acta* **2020**, *187*, 545. [CrossRef]
42. Lettieri, M.; Palladino, P.; Scarano, S.; Minunni, M. Protein-templated copper nanoclusters for fluorimetric determination of human serum albumin. *Microchimic. Acta* **2021**, *188*, 1–9. [CrossRef]
43. Tang, T.; Ouyang, J.; Hu, L.; Guo, L.; Yang, M.; Chen, X. Synthesis of peptide templated copper nanoclusters for fluorometric determination of Fe(III) in human serum. *Microchimic. Acta* **2016**, *183*, 2831–2836. [CrossRef]
44. Fang, J.; Zhang, B.; Yao, Q.; Yang, Y.; Xie, J.; Yan, N. Recent advances in the synthesis and catalytic applications of ligand-protected, atomically precise metal nanoclusters. *Coord. Chem. Rev.* **2016**, *322*, 1–29. [CrossRef]
45. Kardar, Z.S.; Shemirani, F.; Zadmard, R. Determination of iron(II) and iron(III) via static quenching of the fluorescence of tryptophan-protected copper nanoclusters. *Mikrochim. Acta* **2020**, *187*, 81. [CrossRef] [PubMed]
46. Xie, Y.-P.; Shen, Y.-L.; Duan, G.-X.; Han, J.; Zhang, L.-P.; Lu, X. Silver nanoclusters: Synthesis, structures and photoluminescence. *Mater. Chem. Front.* **2020**, *4*, 2205–2222. [CrossRef]
47. Si, H.; Shu, T.; Du, X.; Su, L.; Zhang, X. An Overview on Coinage Metal Nanocluster-Based Luminescent Biosensors via Etching Chemistry. *Biosensors* **2022**, *12*, 511. [CrossRef]
48. Li, Q.; Li, Y.; Li, H.; Yan, X.; Han, G.; Chen, F.; Song, Z.; Zhang, J.; Fan, W.; Yi, C.; et al. Highly Luminescent Copper Nanoclusters Stabilized by Ascorbic Acid for the Quantitative Detection of 4-Aminoazobenzene. *Nanomaterials* **2020**, *10*, 531. [CrossRef]
49. Yang, J.; Pang, R.; Song, D.; Li, M.B. Tailoring silver nanoclusters via doping: Advances and opportunities. *Nanoscale Adv.* **2021**, *3*, 2411–2422. [CrossRef] [PubMed]
50. Qing, T.; Zhang, K.; Qing, Z.; Wang, X.; Long, C.; Zhang, P.; Hu, H.; Feng, B. Recent progress in copper nanocluster-based fluorescent probing: A review. *Mikrochim. Acta* **2019**, *186*, 670. [CrossRef] [PubMed]
51. Zhang, D.; Fang, Y.; Miao, Z.; Ma, M.; Du, X.; Takahashi, S.; Anzai, J.-i.; Chen, Q. Direct electrodeposion of reduced graphene oxide and dendritic copper nanoclusters on glassy carbon electrode for electrochemical detection of nitrite. *Electrochim. Acta* **2013**, *107*, 656–663. [CrossRef]
52. Liu, X.; Shao, C.; Chen, T.; He, Z.; Du, G. Stable silver nanoclusters with aggregation-induced emission enhancement for detection of aluminum ion. *Sens. Actuat B-Chem.* **2019**, *278*, 181–189. [CrossRef]
53. Zhang, C.; Shao, C.; Wang, J.; Li, Z.; Liang, M.; Wang, Y.; Liu, D.; Lu, S. Multifunctional Fluorescent Copper Nanoclusters for Ag^{+} Sensing, Anticounterfeiting, and Blue/White Light-Emitting Diodes. *ACS Appl. Nano Mater.* **2022**, *5*, 7449–7459. [CrossRef]
54. Shao, C.; Li, C.; Zhang, C.; Ni, Z.; Liu, X.; Wang, Y. Novel synthesis of orange-red emitting copper nanoclusters stabilized by methionine as a fluorescent probe for norfloxacin sensing. *Spectrochim. Acta A Mol. Biomol. Spectrosc.* **2020**, *236*, 118334. [CrossRef]
55. Cao, X.; Shao, C.; Zhang, C.; Liang, M.; Wang, Y.; Cheng, J.; Lu, S. Yeast powder derived carbon quantum dots for dopamine detection and living cell imaging. *Anal. Methods* **2022**, *14*, 1342–1350. [CrossRef] [PubMed]

56. Li, C.; Shao, C.; Li, L.; Liu, X.; Liu, M. In situ fabrication of a luminescent copper nanocluster/eggshell membrane composite and its application in visual detection of Ag^+ ions, light-emitting diodes and surface patterning. *Photoch. Photobiol. Sci.* **2019**, *18*, 2942–2951. [CrossRef]
57. Hu, X.; Liu, T.; Zhuang, Y.; Wang, W.; Li, Y.; Fan, W.; Huang, Y. Recent advances in the analytical applications of copper nanoclusters. *Trac-Trend Anal. Chem.* **2016**, *77*, 66–75. [CrossRef]
58. Pan, M.-C.; Lei, Y.-M.; Chai, Y.-Q.; Yuan, R.; Zhuo, Y. In situ controllable generation of copper nanoclusters confined in a poly-L-cysteine porous film with enhanced electrochemiluminescence for alkaline phosphatase detection. *Anal. Chem.* **2020**, *92*, 13581–13587. [CrossRef]
59. Fang, L.; Wang, S.; Song, C.; Lu, S.; Yang, X.; Qi, X.; Liu, H. Boosting nitrate electroreduction to ammonia via in situ generated stacking faults in oxide-derived copper. *Chem. Eng. J.* **2022**, *446*, 137341. [CrossRef]
60. Ruiyi, L.; Huiying, W.; Xiaoyan, Z.; Xiaoqing, L.; Xiulan, S.; Zaijun, L. D-Penicillamine and bovine serum albumin co-stabilized copper nanoclusters with remarkably enhanced fluorescence intensity and photostability for ultrasensitive detection of Ag^+. *New J. Chem.* **2016**, *40*, 732–739. [CrossRef]
61. Long, T.; Guo, Y.; Lin, M.; Yuan, M.; Liu, Z.; Huang, C. Optically active red-emitting Cu nanoclusters originating from complexation and redox reaction between copper (II) and D/L-penicillamine. *Nanoscale* **2016**, *8*, 9764–9770. [CrossRef]
62. Lin, S.; Dong, J.; Zhang, B.; Yuan, Z.; Lu, C.; Han, P.; Xu, J.; Jia, L.; Wang, L. Synthesis of bifunctional fluorescent nanohybrids of carbon dots–copper nanoclusters via a facile method for Fe^{3+} and Tb^{3+} ratiometric detection. *Anal. Methods* **2021**, *13*, 3577–3584. [CrossRef]
63. Li, G.; Luo, Y. Preparation and Characterization of Dendrimer-Templated Ag−Cu Bimetallic Nanoclusters. *Inorg. Chem.* **2008**, *47*, 360–364. [CrossRef] [PubMed]
64. Koyappayil, A.; Kim, H.T.; Lee, M.-H. An efficient and rapid synthesis route to highly fluorescent copper microspheres for the selective and sensitive excitation wavelength-dependent dual-mode sensing of NADH. *Sens. Actuators B Chem.* **2021**, *327*, 128887. [CrossRef]
65. Mu, J.; Peng, Y.; Shi, Z.; Zhang, D.; Jia, Q. Copper nanocluster composites for analytical (bio)-sensing and imaging: A review. *Mikrochim. Acta* **2021**, *188*, 384. [CrossRef]
66. Yaqoob, A.A.; Umar, K.; Ibrahim, M.N.M. Silver nanoparticles: Various methods of synthesis, size affecting factors and their potential applications–a review. *Appl. Nanosci.* **2020**, *10*, 1369–1378. [CrossRef]
67. Pandit, S.; Kundu, S. pH-Dependent reversible emission behaviour of lysozyme coated fluorescent copper nanoclusters. *J. Lumin* **2020**, *228*, 117607. [CrossRef]
68. Yang, Y.; Wei, Q.; Zou, T.; Kong, Y.; Su, L.; Ma, D.; Wang, Y. Dual-emission ratiometric fluorescent detection of dinotefuran based on sulfur-doped carbon quantum dots and copper nanocluster hybrid. *Sens. Actuators B Chem.* **2020**, *321*. [CrossRef]
69. Peng, S.-K.; Yang, H.; Luo, D.; Xie, M.; Tang, W.-J.; Ning, G.-H.; Li, D. Enhancing photoluminescence efficiency of atomically precise copper(i) nanoclusters through a solvent-induced structural transformation. *Inorg. Chem. Front* **2022**, *9*, 5327–5334. [CrossRef]
70. Islam, M.M.; Hu, Z.; Wang, Q.; Redshaw, C.; Feng, X. Pyrene-based aggregation-induced emission luminogens and their applications. *Mater. Chem. Front.* **2019**, *3*, 762–781. [CrossRef]
71. Shao, C.; Xiong, S.; Cao, X.; Zhang, C.; Luo, T.; Liu, G. Dithiothreitol-capped red emitting copper nanoclusters as highly effective fluorescent nanoprobe for cobalt (II) ions sensing. *Microchem. J.* **2021**, *163*, 105922. [CrossRef]
72. Tanwar, A.S.; Meher, N.; Adil, L.R.; Iyer, P.K. Stepwise elucidation of fluorescence based sensing mechanisms considering picric acid as a model analyte. *Analyst* **2020**, *145*, 4753–4767. [CrossRef] [PubMed]
73. Guo, Y.; Shi, S.; Fan, C.; Jin, D. Fluorescent determination of fluazinam with polyethyleneimine-capped copper nanoclusters. *Chem. Phys. Lett.* **2020**, *754*, 137748. [CrossRef]
74. Xue, R.; Geng, X.; Liang, F.; Liu, Y.; Yang, W.; Huang, Z. Natural plant compounds in synthesis and luminescence modulation of metal nanoclusters: Toward sustainable nanoprobes for sensing and bioimaging. *Mater. Today Adv.* **2022**, *16*, 100279. [CrossRef]
75. Zhang, Y.; Deng, Q.; Tang, C.; Zhang, M.; Huang, Z.; Cai, Z. Fluorescent folic acid-capped copper nanoclusters for the determination of rifampicin based on inner filter effect. *Spectrochim. Acta A Mol. Biomol. Spectrosc.* **2023**, *286*, 121944. [CrossRef] [PubMed]
76. Zhao, C.; Jiao, Y.; Gao, Z.; Yang, Y.; Li, H. N, S co-doped carbon dots for temperature probe and the detection of tetracycline based on the inner filter effect. *J. Photoch. Photobio. A* **2018**, *367*, 137–144. [CrossRef]
77. Zheng, X.; Chen, Q.; Zhang, Z.; Wang, Z.; Gong, Z. An aggregation-induced emission copper nanoclusters fluorescence probe for the sensitive detection of tetracycline. *Microchem. J.* **2022**, *180*, 107570. [CrossRef]
78. Sivakumar, R.; Lee, N.Y. Recent progress in smartphone-based techniques for food safety and the detection of heavy metal ions in environmental water. *Chemosphere* **2021**, *275*, 130096. [CrossRef]
79. Zhang, M.; Cui, X.; Li, N. Smartphone-based mobile biosensors for the point-of-care testing of human metabolites. *Mater. Today Bio.* **2022**, *14*, 100254. [CrossRef]
80. Fernandes, G.M.; Silva, W.R.; Barreto, D.N.; Lamarca, R.S.; Lima Gomes, P.C.F.; da Silveira Petruci, J.F.; Batista, A.D. Novel approaches for colorimetric measurements in analytical chemistry—A review. *Anal. Chim. Acta* **2020**, *1135*, 187–203. [CrossRef]
81. Yan, Z.; Cai, Y.; Zhang, J.; Zhao, Y. Fluorescent sensor arrays for metal ions detection: A review. *Measurement* **2022**, *187*, 110355. [CrossRef]

82. Fu, L.; Wang, A.; Xie, K.; Zhu, J.; Chen, F.; Wang, H.; Zhang, H.; Su, W.; Wang, Z.; Zhou, C.; et al. Electrochemical detection of silver ions by using sulfur quantum dots modified gold electrode. *Sens. Actuators B Chem.* **2020**, *304*, 127390. [CrossRef]
83. Xu, G.; Wang, G.; Zhu, Y.; Chen, L.; He, X.; Wang, L.; Zhang, X. Amplified and selective detection of Ag^+ ions based on electrically contacted enzymes on duplex-like DNA scaffolds. *Biosens. Bioelectron.* **2014**, *59*, 269–275. [CrossRef]
84. Kang, J.; Gao, P.; Zhang, G.; Shi, L.; Zhou, Y.; Wu, J.; Shuang, S.; Zhang, Y. Rapid sonochemical synthesis of copper nanoclusters with red fluorescence for highly sensitive detection of silver ions. *Microchem. J.* **2022**, *178*, 107370. [CrossRef]
85. Arthy, M.; Brindha, J.; Viswanathan, S.; Gnanasekar, A.K.; Nanammal, V.; Raju, R.; Al Obaid, S.; Almoallim, H.S.; Selva, A.; Velmurugan, P. Detection of Ag^+ by Synthesizing Fluorescent Copper Nanoparticles through Ultrasensitive Free Label Approach. *J. Nanomater.* **2022**, *2022*, 8642134. [CrossRef]
86. Hu, X.; Zhang, X.; Cao, H.; Huang, Y. Modulating the size and photoluminescence of a copper nanocluster via metal-organic frameworks encapsulating strategy for fluorescence sensing. *Microchem. J.* **2022**, *182*, 107876. [CrossRef]
87. Yang, D.; Zhou, T.; Tu, Y.; Yan, J. Detection of silver through amplified quenching of fluorescence from polyvinyl pyrrolidone-stabilized copper nanoclusters. *Mikrochim. Acta* **2021**, *188*, 212. [CrossRef]
88. Lu, S.; Gu, Z.; Hummel, M.; Zhou, Y.; Wang, K.; Xu, B.B.; Wang, Y.; Li, Y.; Qi, X.; Liu, X. Nickel Oxide Immobilized on the Carbonized Eggshell Membrane for Electrochemical Detection of Urea. *J. Electrochem. Soc.* **2020**, *167*, 106509. [CrossRef]
89. Lu, S.; Hummel, M.; Kang, S.; Pathak, R.; He, W.; Qi, X.; Gu, Z. Density Functional Theory Investigation of the NiO@Graphene Composite as a Urea Oxidation Catalyst in the Alkaline Electrolyte. *ACS Omega.* **2021**, *6*(22), 14648–14654. [CrossRef]
90. Lu, S.; Hummel, M.; Gu, Z.; Wang, Y.; Wang, K.; Pathak, R.; Zhou, Y.; Jia, H.; Qi, X.; Zhao, X.; et al. Highly Efficient Urea Oxidation via Nesting Nano-Nickel Oxide in Eggshell Membrane-Derived Carbon. *ACS Sustain. Chem. Eng.* **2021**, *9*, 1703–1713. [CrossRef]
91. Wang, Y.; Zhang, L.; Han, X.; Zhang, L.; Wang, X.; Chen, L. Fluorescent probe for mercury ion imaging analysis: Strategies and applications. *Chem. Eng. J.* **2021**, *406*, 127166. [CrossRef]
92. Bernhoft, R.A. Mercury toxicity and treatment: A review of the literature. *J. Environ. Public Health.* **2012**, *2012*, 460508. [CrossRef]
93. Li, L.; Huang, M.; Liu, X.; Sun, D.; Shao, C. In Situ Generation of Fluorescent Copper Nanoclusters Embedded in Monolithic Eggshell Membrane: Properties and Applications. *Materials* **2018**, *11*, 1913. [CrossRef]
94. Maruthupandi, M.; Thiruppathi, D.; Vasimalai, N. One minute synthesis of green fluorescent copper nanocluster: The preparation of smartphone aided paper-based kit for on-site monitoring of nanomolar level mercury and sulfide ions in environmental samples. *J. Hazard. Mater.* **2020**, *392*, 122294. [CrossRef]
95. Bhamore, J.R.; Deshmukh, B.; Haran, V.; Jha, S.; Singhal, R.K.; Lenka, N.; Kailasa, S.K.; Murthy, Z.V.P. One-step eco-friendly approach for the fabrication of synergistically engineered fluorescent copper nanoclusters: Sensing of Hg^{2+} ion and cellular uptake and bioimaging properties. *New J. Chem.* **2018**, *42*, 1510–1520. [CrossRef]
96. Li, Z.; Pang, S.; Wang, M.; Wu, M.; Li, P.; Bai, J.; Yang, X. Dual-emission carbon dots-copper nanoclusters ratiometric photoluminescent nano-composites for highly sensitive and selective detection of Hg^{2+}. *Ceram. Int.* **2021**, *47*, 18238–18245. [CrossRef]
97. Pang, J.; Xie, R.; Chua, S.; Zou, Y.; Tang, M.; Zhang, F.; Chai, F. Preparation of fluorescent bimetallic silver/copper nanoparticles and their utility of dual-mode fluorimetric and colorimetric probe for Hg^{2+}. *Spectrochim. Acta A Mol. Biomol. Spectrosc.* **2021**, *261*, 120035. [CrossRef] [PubMed]
98. Liang, M.; Shao, C.; Zhang, Q.; Zhang, C.; Wang, Y.; Zheng, X.; Lu, S. High-Performance Formaldehyde Sensing Using Paper-Based Fluorescent Copper Nanoclusters. *IEEE Sens. J.* **2023**, *23*, 2076–2084. [CrossRef]
99. Chiang, T.H.; Hsiao, H.H. Single drop analysis of mercury ions by rational design of peptide coated gold nanoparticles integrated with MALDI-MS measurement. *Talanta* **2023**, *253*, 123913. [CrossRef]
100. Zhang, C.; Liang, M.; Shao, C.; Li, Z.; Cao, X.; Wang, Y.; Wu, Y.; Lu, S. Visual Detection and Sensing of Mercury Ions and Glutathione Using Fluorescent Copper Nanoclusters. *ACS Appl. Bio Mater.* **2023**. [CrossRef] [PubMed]
101. Shojaeifard, Z.; Heidari, N.; Hemmateenejad, B. Bimetallic AuCu nanoclusters-based florescent chemosensor for sensitive detection of Fe^{3+} in environmental and biological systems. *Spectrochim. Acta A Mol. Biomol. Spectrosc.* **2019**, *209*, 202–208. [CrossRef] [PubMed]
102. Kalaiyarasan, G.; Joseph, J.; Kumar, P. Phosphorus-Doped Carbon Quantum Dots as Fluorometric Probes for Iron Detection. *ACS Omega* **2020**, *5*, 22278–22288. [CrossRef]
103. Wang, Y.; Jian, J.; Sun, B.; Wei, Y.; Pan, D.; Cao, J.; Shen, Y. Engineering of onsite point-of-care testing of Fe^{3+} with visual ratiometric fluorescent signals of copper nanoclusters-driven portable smartphone. *Sensor Actuators B-Chem.* **2022**, *370*, 132413. [CrossRef]
104. Tai, Y.-T.; Simon, T.; Chu, Y.-Y.; Ko, F.-H. One-pot synthesis of copper nanoconjugate materials as luminescent sensor for Fe^{3+} and I^- detection in human urine sample. *Sens. Bio-Sens. Res.* **2020**, *27*, 100319. [CrossRef]
105. Wuri, H.; Ai, J.; Ga, L. Template method synthesis of highly fluorescent duplex oligonucleotide copper nanomaterials for Fe^{3+} sensing. *Mater. Res. Express* **2020**, *7*, 125001. [CrossRef]
106. Singh, R.; Majhi, S.; Sharma, K.; Ali, M.; Sharma, S.; Choudhary, D.; Tripathi, C.S.P.; Guin, D. BSA stabilized copper nanoclusters as a highly sensitive and selective probe for fluorescence sensing of Fe^{3+} ions. *Chem. Phys. Lett* **2022**, *787*. [CrossRef]
107. Ke, B.; Ma, L.; Kang, T.; He, W.; Gou, X.; Gong, D.; Du, L.; Li, M. In Vivo Bioluminescence Imaging of Cobalt Accumulation in a Mouse Model. *Anal. Chem.* **2018**, *90*, 4946–4950. [CrossRef]
108. Zhao, R.X.; Liu, A.Y.; Wen, Q.L.; Wu, B.C.; Wang, J.; Hu, Y.L.; Pu, Z.F.; Ling, J.; Cao, Q. Glutathione stabilized green-emission gold nanoclusters for selective detection of cobalt ion. *Spectrochim. Acta A Mol. Biomol. Spectrosc.* **2021**, *254*, 119628. [CrossRef] [PubMed]

109. Han, B.-Y.; Hu, X.-X.; Xu, J.; He, G.-H. Lysozyme-Directed Synthesis of Yellow-Emitting Copper Nanoclusters for Cobalt Ions (Co^{2+}) Sensing. *J. Nanosci. Nanotechno.* **2018**, *18*, 7933–7938. [CrossRef]
110. Huang, M.; Tong, C. Silicon nanoparticles / gold nanoparticles composite as a fluorescence probe for sensitive and selective detection of Co^{2+} and vitamin B_{12} based on the selective aggregation and inner filter effect. *Spectrochim. Acta A Mol. Biomol. Spectrosc.* **2022**, *268*, 120706. [CrossRef]
111. Lin, Y.S.; Chiu, T.C.; Hu, C.C. Fluorescence-tunable copper nanoclusters and their application in hexavalent chromium sensing. *RSC Adv.* **2019**, *9*, 9228–9234. [CrossRef] [PubMed]
112. Han, B.; Xiang, R.; Hou, X.; Yu, M.; Peng, T.; Li, Y.; He, G. One-step rapid synthesis of single thymine-templated fluorescent copper nanoclusters for "turn on" detection of Mn^{2+}. *Anal. Methods* **2017**, *9*, 2590–2595. [CrossRef]
113. Bai, H.; Tu, Z.; Liu, Y.; Tai, Q.; Guo, Z.; Liu, S. Dual-emission carbon dots-stabilized copper nanoclusters for ratiometric and visual detection of $Cr_2O_7^{2-}$ ions and Cd^{2+} ions. *J. Hazard Mater.* **2020**, *386*, 121654. [CrossRef] [PubMed]
114. Rasheed, T.; Bilal, M.; Nabeel, F.; Iqbal, H.M.N.; Li, C.; Zhou, Y. Fluorescent sensor based models for the detection of environmentally-related toxic heavy metals. *Sci. Total. Environ.* **2018**, *615*, 476–485. [CrossRef] [PubMed]
115. Nain, A.; Tseng, Y.-T.; Lin, Y.-S.; Wei, S.-C.; Mandal, R.P.; Unnikrishnan, B.; Huang, C.-C.; Tseng, F.-G.; Chang, H.-T. Tuning the photoluminescence of metal nanoclusters for selective detection of multiple heavy metal ions. *Sens. Actuators B Chem.* **2020**, *321*. [CrossRef]
116. Benavides, J.; Quijada-Garrido, I.; Garcia, O. The synthesis of switch-off fluorescent water-stable copper nanocluster Hg^{2+} sensors via a simple one-pot approach by an in situ metal reduction strategy in the presence of a thiolated polymer ligand template. *Nanoscale* **2020**, *12*, 944–955. [CrossRef]

Disclaimer/Publisher's Note: The statements, opinions and data contained in all publications are solely those of the individual author(s) and contributor(s) and not of MDPI and/or the editor(s). MDPI and/or the editor(s) disclaim responsibility for any injury to people or property resulting from any ideas, methods, instructions or products referred to in the content.